



ANALYSIS OF SEXTANT NAVIGATION MEASUREMENTS
DURING LUNAR MODULE RENDEZVOUS

By T. B. Murtagh

Manned Spacecraft Center
Houston, Texas

NATIONAL AERONAUTICS AND SPACE ADMINISTRATION

For sale by the Clearinghouse for Federal Scientific and Technical Information
Springfield, Virginia 22151 - CFSTI price \$3.00

ABSTRACT

Two methods are presented in this document for optimizing individual spacecraft-star navigation measurements along the nominal concentric flight plan rendezvous trajectory for the Apollo program. In the first method, a star is selected which will minimize the relative root-mean-square position errors at the measurement time. In the second method, a star is selected which will lie closest to the measurement plane defined by the inertial position vectors of the Command Service Module and the Lunar Module. These spacecraft-star measurements are made up to the circularization maneuver; thereafter only spacecraft-lunar horizon measurements are made. Both measurement types are processed using a Kalman filter which simultaneously solves for relative Lunar Module-Command Service Module state, inertial Command Service Module state, and the sextant bias. The results of the study indicate that fewer stars are required for the second method outlined, and that both methods produce comparable uncertainties at rendezvous.

CONTENTS

Section	Page
SUMMARY	1
INTRODUCTION	1
SYMBOLS	2
ANALYSIS	5
Description of Navigation System	5
Measurement Types	5
Optimum Star Selection	6
Assumptions	6
Description of Simulation	7
RESULTS AND DISCUSSION	7
Trajectory Constraints and Navigation Measurements	7
Effect of No Measurements	8
Stars Chosen to Minimize Total Relative Root-Mean-Square Position Error	8
Stars Chosen Nearest the Measurement Plane	8
Effect of CSM-Horizon Measurements	9
CONCLUDING REMARKS	9
APPENDIX A - NAVIGATION SYSTEM EQUATIONS	10
APPENDIX B - SENSITIVITY VECTORS FOR SPACECRAFT-STAR AND SPACECRAFT-HORIZON MEASUREMENT TYPES	13
APPENDIX C - NUMERICAL OPTIMIZATION TECHNIQUE FOR STAR SELECTION	15
REFERENCES	16

TABLES

Table		Page
I	ABBREVIATED 20-STAR CATALOGUE USED WITH DIGITAL COMPUTER SIMULATION	17
II	COMPARISON OF UNCERTAINTIES AT RENDEZVOUS – SPACECRAFT-HORIZON MEASUREMENTS PROCESSED AFTER CIRCULARIZATION AND NOT PROCESSED AFTER CIRCULARIZATION	18

FIGURES

Figure		Page
1	Geometry of spacecraft-star included angle measurement	19
2	Geometry of spacecraft-lunar horizon included angle measurement	19
3	Basic geometry of the nominal concentric flight plan rendezvous trajectory	20
4	No measurements processed from burnout to rendezvous	
	(a) Relative altitude error	21
	(b) Relative range error	22
	(c) Relative track error	23
5	No measurements processed from burnout to rendezvous	
	(a) Relative altitude rate error	24
	(b) Relative range rate error	25
	(c) Relative track rate error	26
6	Spacecraft-star measurements choosing stars to minimize total relative rms position processed every 2 minutes up to circularization; spacecraft-lunar horizon measurements processed thereafter	
	(a) Relative altitude error	27
	(b) Relative range error	28
	(c) Relative track error	29
7	Spacecraft-star measurements choosing stars to minimize total relative rms position processed every 2 minutes up to circularization; spacecraft-lunar horizon measurements processed thereafter	
	(a) Relative altitude rate error	30
	(b) Relative range rate error	31
	(c) Relative track rate error	32
8	Spacecraft-star measurements choosing stars to minimize total relative rms position processed every 6 minutes up to circularization; spacecraft-lunar horizon measurements processed thereafter	
	(a) Relative altitude error	33
	(b) Relative range error	34
	(c) Relative track error	35

Figure		Page
9	Spacecraft-star measurements choosing stars to minimize total relative rms position processed every 6 minutes up to circularization; spacecraft-lunar horizon measurements processed thereafter	
	(a) Relative altitude rate error	36
	(b) Relative range rate error	37
	(c) Relative track rate error	38
10	Spacecraft-star measurements choosing stars nearest the measurement plane processed every 2 minutes up to circularization; spacecraft-lunar horizon measurements processed thereafter	
	(a) Relative altitude error	39
	(b) Relative range error	40
	(c) Relative track error	41
11	Spacecraft-star measurements choosing stars nearest the measurement plane processed every 2 minutes up to circularization; spacecraft-lunar horizon measurements processed thereafter	
	(a) Relative altitude rate error	42
	(b) Relative range rate error	43
	(c) Relative track rate error	44
12	Spacecraft-star measurements choosing stars nearest the measurement plane processed every 6 minutes up to circularization; spacecraft-lunar horizon measurements processed thereafter	
	(a) Relative altitude error	45
	(b) Relative range error	46
	(c) Relative track error	47
13	Spacecraft-star measurements choosing stars nearest the measurement plane processed every 6 minutes up to circularization; spacecraft-lunar horizon measurements processed thereafter	
	(a) Relative altitude rate error	48
	(b) Relative range rate error	49
	(c) Relative track rate error	50

ANALYSIS OF SEXTANT NAVIGATION MEASUREMENTS

DURING LUNAR MODULE RENDEZVOUS

By T. B. Murtagh
Manned Spacecraft Center

SUMMARY

Two methods are presented in this document for optimizing individual spacecraft-star navigation measurements along the nominal concentric flight plan rendezvous trajectory for the Apollo program. In the first method, a star is selected which will minimize the relative root-mean-square position errors at the measurement time. In the second method, a star is selected which will lie closest to the measurement plane defined by the inertial position vectors of the Command Service Module and the Lunar Module. These spacecraft-star measurements are made at specified intervals up to the circularization maneuver. Thereafter, only spacecraft-lunar horizon measurements are made, assuming a 1/2-nautical mile lunar-horizon uncertainty. Both measurement types are processed using a Kalman filter which simultaneously solves for relative Lunar Module-Command Service Module state, for inertial Command Service Module state, and for the sextant bias. Although this does not simulate the filter planned for the rendezvous phase of the Apollo mission, the inclusion of the Command Service Module inertial state errors was necessary to present a realistic error analysis of the handheld space sextant as a backup navigational aid during rendezvous. Each of the measurement types is assumed to be made using a handheld space sextant with an overall accuracy of 30 arc seconds and an initial 60-arc-second bias. The results of the study indicate that fewer stars are required for the second method outlined above. Both methods produce comparable uncertainties at rendezvous. For the cases considered, these uncertainties in total root-mean-square relative position and velocity were of the order of 0.25 nautical mile and 2.0 fps.

INTRODUCTION

During the Lunar Module-Command Service Module (LM/CSM) rendezvous phase of the Apollo Lunar Landing Mission, navigation of the Lunar Module (LM) will be based upon observations of the Command Service Module (CSM). The primary guidance and navigation system will utilize either rendezvous radar range and range-rate measurements or optical tracker azimuth and elevation measurements of the line of sight between the two vehicles as input to the guidance equations to control the mid-course and terminal phases of the rendezvous maneuver. In either case, the tracking unit is capable of providing automatic relative position data and/or velocity data

typically processed on board at 1-minute intervals. As a backup to the primary guidance and navigation (G&N) system, the handheld space sextant is currently being considered to provide manual tracking of the CSM during the rendezvous maneuvers in the event of a failure of the onboard automatic tracking unit.

Two types of measurements utilizing the sextant and involving CSM observation are the CSM-star and CSM-horizon included angle measurements. The first type can be optimized by the judicious choice of the star to be involved; the second type can be optimized only insofar as either the earth horizon or the lunar horizon can be chosen (provided that the earth is visible). In this study only the lunar horizon was used.

Many criteria can be used in choosing the star involved in the measurement. In this paper only two criteria were employed. The first involved selection of a star which would minimize the total relative root-mean-square (rms) position uncertainty at the measurement time. The second would select a star nearest to the measurement plane. This plane is defined by the inertial position vectors of the CSM and LM at each measurement time.

This study attempts to present a realistic evaluation of the handheld space sextant as a backup navigational aid during rendezvous. The study also presents two methods of optimizing individual spacecraft-star measurements using the nominal concentric flight-plan rendezvous trajectory.

A digital computer program (NAVIGATE) was used to simulate the dynamics of the problem as well as to process the optical measurements by using a Kalman filter. As previously mentioned, this filter simultaneously solves for the relative LM/CSM state, the inertial CSM state, and the sextant bias to partially account for the uncertainty in the command module orbit. Although this does not simulate the filter planned for the rendezvous phase of the Apollo mission, the inclusion of the CSM uncertainties was necessary to present a more realistic error analysis of sextant performance as a navigation sensor.

SYMBOLS

C	scalar defined by equation (A8)
$E(t)$	covariance matrix of state estimation errors
$E(t_0)$	covariance matrix defined by equation (A1)
E_{β}	variance of sextant bias estimation errors
\bar{e}_0	initial error in estimate of inertial CSM position vector
$\bar{e}(t)$	error in estimate of inertial CSM position vector
$F(t)$	matrix defined by equation (A3)

G_{CL}	gradient of gravity with respect to position derived from relative LM/CSM equations of motion
G_{CSM}	gradient of gravity with respect to position derived from CSM equations of motion
$H(t)$	sensitivity vector defined by equation (B1)
I	three-by-three identity matrix
$K(t)$	weight vector defined by equation (A6)
$M(t)$	scalar defined by equation (A7)
P_i	parameter defined by equation (C2)
$Q_E(t)$	expected value of included angle computed from current estimate of state vector
$R(t)$	scalar defined by equation (A9)
\bar{r}_{CSM}	inertial CSM position vector
r_{LM}	magnitude of inertial LM position vector
\bar{r}_{LM}	inertial LM position vector
r_{moon}	magnitude of moon radius
r_p	magnitude of planet radius
\bar{r}_s^0	unit vector to star
t_M	measurement time
$W(t)$	matrix defined by $E(t) = W(t)W^T(t)$
$\bar{W}^*(t)$	updated matrix defined by equation (A5)
$\hat{X}(t)$	state vector estimate extrapolated to measurement time

$\overset{*}{\bar{X}}(t)$	updated estimate of state vector defined by equation (A4)
\bar{a}	vector defined by equation (B2)
\bar{a}_1	vector defined by equation (B4)
β	angle between $\bar{\rho}_{cl}$ and lunar horizon line (fig. 2)
$\bar{\beta}$	vector defined by equation (B2)
$\bar{\beta}_1$	vector defined by equation (B3) or (B5)
γ	angle between lunar horizon line and \bar{r}_{LM} (fig. 2)
ΔQ	difference between value of included angle actually measured and the expected value of the angle computed from current estimate of state vector
$\Delta \hat{W}_i$	parameter defined in equation (C1)
$\bar{\delta}_0$	initial error in estimate of inertial CSM velocity vector
$\bar{\delta}(t)$	error in estimate of inertial CSM velocity vector
$\bar{\epsilon}_0$	initial error in estimate of relative LM/CSM position vector
$\bar{\epsilon}(t)$	error in estimate of relative LM/CSM position vector
$\bar{\eta}_0$	initial error in estimate of relative LM/CSM velocity vector
$\bar{\eta}(t)$	error in estimate of relative LM/CSM velocity vector
Φ	angle between \bar{r}_s^0 and $\bar{\rho}_{cl}$ (fig. 1)
ρ_{cl}	magnitude of relative LM/CSM position vector
$\bar{\rho}_{cl}$	relative LM/CSM position vector

- σ_H^2 horizon variance
- σ_I^2 sextant variance
- σ_T^2 total variance defined by equation (A9)
- $\nabla_{\bar{X}}()$ gradient of () with respect to state vector

Subscripts :

- 0 initial value
- i 1, 2, ..., 20 stars

Superscripts :

- T transpose

Operators :

- ($\dot{}$) derivative of () with respect to time
- ($\hat{}$) estimate of ()

ANALYSIS

Description of Navigation System

The pertinent navigation system equations are developed and presented in appendix A. The state variables employed in the simulated minimum variance estimator are the inertial position and velocity of the CSM, the relative position and velocity of the LM with respect to the CSM, and the sextant bias. With this estimation scheme, both the inertial CSM errors and the bias errors can be determined. Other error sources could be accounted for in the state variable array, but these two error sources are the primary ones to be considered, with others second order by comparison.

Measurement Types

The two measurement types considered in this study, adaptable to an optical device such as the handheld space sextant described in reference 1, are the spacecraft-star and spacecraft-horizon included angle measurements. The geometry

of the spacecraft-star measurement is illustrated in figure 1, and the spacecraft-horizon geometry is presented in figure 2. In this study, only spacecraft-lunar horizon measurements are employed, although spacecraft-earth horizon measurements are possible if the earth is visible. The angles ϕ and β , defined in figures 1 and 2, respectively, are the measurement parameters incorporated into the filter equations. The sensitivity vectors for each of these measurement types relate measurement deviations to relative state deviations and are developed and presented in appendix B.

Optimum Star Selection

Two methods were utilized to select the star involved in the CSM-star included angle measurement. In the first method, a star was selected which minimized the total rms relative position uncertainty at the measurement time. For the ideal case of zero sensor random errors this implies the selection of a star which would produce a sensitivity vector parallel to the principal eigenvector of the covariance matrix at the time of the measurement (see ref. 2).

In the second method, the selected star was nearest the plane defined by the inertial position vectors of the CSM and the LM at each measurement time. The numerical optimization technique employed in implementing the above criteria is discussed in appendix C.

Assumptions

1. The nominal concentric flight-plan rendezvous trajectory (ref. 3) was used to generate the results presented in this paper. The basic geometry of this trajectory is illustrated in figure 3. All maneuvers were assumed to be impulsive.
2. The assumed random error for the combined optical system (sextant, astronaut, and spacecraft window) was 30 arc seconds; the initial estimate of the sextant bias was assumed to be 60 arc seconds.
3. The uncertainty in defining the lunar horizon was assumed to be 1/2 nautical mile. The model used to compute the total optical system variance when processing spacecraft-lunar horizon measurements is given in appendix A.
4. The angle between the line of sight to the CSM and the line of sight to either a star or the lunar horizon was not allowed to exceed an assumed field-of-view constraint of 50° .
5. The initial covariance matrix of the CSM inertial state estimation errors was diagonal with total rms position and velocity errors equal to 1500 ft and 1.0 fps. The initial covariance matrix of the LM inertial state estimation errors was obtained by an analysis of the powered phase of the LM ascent from the lunar surface. The sum of the initial CSM and LM inertial covariance matrices was then used to represent the initial relative LM/CSM covariance matrix. The resulting total initial relative rms position and velocity errors were 3000 ft and 9.9 fps.

Description of Simulation

A digital computer simulation (NAVIGATE) was used to generate the results presented in this document. The basic components of this simulation are a precision numerical integrator, a star and planet ephemeris, a Gaussian random number generator, and a Kalman Linear Filter for processing sensor data.

The equations of motion are derived on the basis of including the gravitational effects of the moon on the vehicle, including tri-axiality perturbations, and a spherical and homogeneous sun and earth. The position and velocity of the spacecraft are numerically integrated in an inertial rectangular coordinate system with the x- and y-axes in a plane parallel to the earth equatorial plane. The positive x-axis is taken in the direction of the first point of Aries, the z-axis is parallel to the earth polar axis, and the y-axis completes the orthogonal right-hand triad.

A star and planet ephemeris is also a part of the integrator package, capable of generating unit vectors to any one of approximately 1500 stars given a time and some state vector in inertial space. The calculation of appropriate planet positions at this specified time then determines whether a particular star is visible. For this study an abbreviated star catalogue was used which consists of 20 stars chosen from the 54-star catalogue set up in the Apollo Guidance Computer for inertial platform alignment (see table I). The right ascensions and declinations given in this table are mean values for a 1963.0 epoch.

The Gaussian random number generator is used to compute initial random error vectors using the eigenvalues and eigenvectors of the initial covariance matrix of state estimation errors. These random error vectors are then added to the initial actual state vector to calculate a simulated onboard estimated state vector.

Finally, the Kalman Linear Filter equations are used to propagate and update the initial covariance matrix of state estimation errors and to process the included angle data from the sextant. The rms position and velocity errors, computed from the square root of the trace of the covariance matrix, are presented as computer output in a locally level inertial coordinate system which displays both in-plane and out-of-plane errors. The x-axis of this coordinate system is along the radius vector to the spacecraft (altitude); the y-axis is in the direction of the velocity (range); and the z-axis is along the orbital angular momentum vector (track). The errors in this system are then designated as altitude, range, or track errors – or their time rate of change – and are presented as such in the graphs which appear in the following pages.

RESULTS AND DISCUSSION

Trajectory Constraints and Navigation Measurements

The epoch time selected is the termination of the powered phase of the LM ascent from the lunar surface (burnout). The final time corresponds to rendezvous (roughly 2.4 hours after burnout). No navigation measurements were processed during the 6 minutes after burnout or during the 20 minutes prior to rendezvous. These constraints were imposed because of other assumed astronaut duties during these intervals.

Since stars will only be visible in darkness, CSM-star measurements were performed only during the interval from 6 minutes after burnout up to the circularization maneuver. After the circularization maneuver, only the CSM-lunar horizon measurements were performed.

Effect of No Measurements

The effect of making no measurements on the relative LM/CSM position and velocity errors from burnout to rendezvous is presented in figures 4 and 5, respectively. The initial altitude and range errors of 0.2 and 0.3 nautical mile rise rather quickly to 7.0 and 41.0 nautical miles, respectively. The track error displays an oscillatory behavior and never exceeds 1.3 nautical miles in the time interval shown. The initial altitude rate and range rate of 3.6 and 6.1 fps also rise to values of 224.0 and 26.0 fps, respectively. The track rate error is also oscillatory, and never exceeds 7.0 fps in the region of interest.

Stars Chosen to Minimize Total Relative Root-Mean-Square Position Error

Time histories of rms relative position and velocity uncertainties for the case of measurements based on stars chosen to minimize the total relative rms position uncertainty at each measurement time are given in figures 6 to 9. The position and velocity uncertainties given in figures 6 and 7, respectively, are based on measurements processed at 2-minute intervals. This schedule resulted in the processing of 38 CSM-star measurements and 10 CSM-lunar horizon measurements. The comparatively small number of horizon measurements processed was because the angle between the line of sight to the CSM and the line of sight to the horizon exceeded the field-of-view constraint previously described. The resulting rms relative altitude, range, and track errors at rendezvous were 0.06, 0.25, and 0.01 nautical mile; the corresponding relative altitude, range and track rate errors were 1.35, 0.20 and 0.06 fps.

Figures 8 and 9 present the rms position and velocity uncertainties processing measurements at 6-minute intervals with the same schedule as described for figures 6 and 7. For this case, 13 spacecraft-star measurements were processed, and only 3 spacecraft-horizon measurements were processed. The altitude, range, and track errors at rendezvous for this case were 0.08, 0.32, and 0.01 nautical mile; the corresponding rate errors were 1.70, 0.31, and 0.07 fps.

From these data it appears that the resulting uncertainties at rendezvous are not too sensitive to the sighting frequency. Also, 9 of the 20 stars in the simulated catalogue were utilized for both cases presented.

Stars Chosen Nearest the Measurement Plane

Time histories of relative rms position and velocity uncertainties of measurements based on stars chosen nearest the measurement plane are given in figures 10 and 11 for the 2-minute schedule, and in figures 12 and 13 for the 6-minute

schedule. For the 2-minute schedule, the resulting rms altitude, range, and track errors at rendezvous were 0.06, 0.25, and 0.01 nautical mile; the corresponding rate errors were 1.36, 0.20, and 0.08 fps. For the 6-minute schedule, the rms position errors (altitude, range, and track components) at rendezvous were 0.07, 0.31, and 0.01 nautical mile; the corresponding rate errors were 1.65, 0.25, and 0.09 fps.

A comparison of these data with the data presented in the previous section indicates that fewer stars were required when the selected stars were nearest to the measurement plane for both measurement intervals. In this case, only four stars were used for both sighting frequencies as opposed to the nine stars required in the previous case.

Effect of CSM-Horizon Measurements

Finally, the above cases were computed again except that no spacecraft-horizon measurements were processed after the circularization maneuver. These results are summarized in table II where a comparison of the uncertainties at rendezvous is displayed both with and without processing sensor measurements after circularization. The horizon measurements made after circularization reduced the uncertainties at rendezvous by a factor of three, compared with the cases where no measurements were made after circularization.

CONCLUDING REMARKS

Two methods for optimizing individual CSM-star navigation measurements along the nominal LM concentric flight plan rendezvous trajectory have been presented. The first method selected stars on the basis of minimizing the total relative rms position errors at each measurement time. The second method selected the star nearest the measurement plane. The CSM-star measurements were processed at specified intervals up to the circularization maneuver; thereafter, only CSM-lunar horizon measurements were processed. The results of the study indicate that fewer stars are required for the second method and that both methods produce comparable errors at rendezvous. The sighting frequency was not critical where the uncertainties at rendezvous were concerned. Also, the CSM-horizon measurements made after circularization reduced the uncertainties at rendezvous by a factor of three when compared with the cases where no measurements were processed after circularization.

National Aeronautics and Space Administration
Manned Spacecraft Center
Houston, Texas, December 7, 1966
981-89-00-00-72

APPENDIX A

NAVIGATION SYSTEM EQUATIONS

In order to update the estimates of relative LM/CSM position and velocity, navigation measurements are required. As part of the navigation technique, certain statistical data must be maintained to assist in the processing of the navigation measurements. If $\bar{e}(t)$ and $\bar{\delta}(t)$ are the errors in the estimates of the inertial CSM position and velocity, respectively, and $\bar{\epsilon}(t)$ and $\bar{\eta}(t)$ are the errors in the estimates of the relative LM/CSM position and velocity, respectively, then the initial 13-dimensional covariance or correlation matrix $E(t_0)$ is defined by

$$E(t_0) = \begin{bmatrix} \overline{e_0 e_0^T} & \overline{e_0 \delta_0^T} & 0 & 0 & 0 \\ \overline{\delta_0 e_0^T} & \overline{\delta_0 \delta_0^T} & 0 & 0 & 0 \\ 0 & 0 & \overline{\epsilon_0 \epsilon_0^T} & \overline{\epsilon_0 \eta_0^T} & 0 \\ 0 & 0 & \overline{\eta_0 \epsilon_0^T} & \overline{\eta_0 \eta_0^T} & 0 \\ 0 & 0 & 0 & 0 & E_\beta \end{bmatrix} \quad (A1)$$

where the zero subscripts denote values at t_0 , and E_β is the variance of the sextant bias estimation errors. However, in order to insure that $E(t)$ will at least remain positive and semidefinite, the substitution $E(t_0) = W(t_0)W^T(t_0)$ is made, and this initial W -matrix is then extrapolated by direct numerical integration of the equation

$$\dot{W}(t) = F(t)W(t) \quad (A2)$$

The 13-dimensional matrix $F(t)$ is defined by

$$F(t) = \begin{bmatrix} 0 & I & 0 & 0 & 0 \\ G_{\text{CSM}} & 0 & 0 & 0 & 0 \\ 0 & 0 & 0 & I & 0 \\ 0 & 0 & G_{\text{CL}} & 0 & 0 \\ 0 & 0 & 0 & 0 & 0 \end{bmatrix} \quad (\text{A3})$$

where I is a three-by-three identity matrix and G_{CSM} and G_{CL} are also three-by-three matrices conventionally referred to as gravity gradient matrices. The elements of these matrices were evaluated from the equations of motion which, for this study, were assumed to include the effects of the moon tri-axiality on the spacecraft motion and the effects of a spherical and homogeneous sun and earth. When a navigation measurement is made, the updated estimate of the state vector is computed from

$$\hat{\mathbf{X}}^*(t) = \hat{\mathbf{X}}(t) + \mathbf{K}(t)\Delta\mathbf{Q} \quad (\text{A4})$$

and that of the W -matrix from

$$\hat{\mathbf{W}}^*(t) = \hat{\mathbf{W}}(t) \left[\mathbf{I} - \frac{\hat{\mathbf{W}}^T(t)\mathbf{H}^T(t)\mathbf{H}(t)\hat{\mathbf{W}}(t)}{\mathbf{M}(t)(1 + C)} \right] \quad (\text{A5})$$

The value of the weight vector $\mathbf{K}(t)$ is chosen optimally so that the mean-squared position and velocity uncertainties are simultaneously minimized. It is defined by the equation

$$\mathbf{K}(t) = \hat{\mathbf{W}}(t)\hat{\mathbf{W}}^T(t)\mathbf{H}^T(t)\mathbf{M}^{-1}(t) \quad (\text{A6})$$

with the matrix $\mathbf{M}(t)$ defined by

$$\mathbf{M}(t) = \mathbf{H}(t)\hat{\mathbf{W}}(t)\hat{\mathbf{W}}^T(t)\mathbf{H}^T(t) + \mathbf{R}(t) \quad (\text{A7})$$

and

$$C = \sqrt{R(t)/M(t)} \quad (A8)$$

For the measurement types considered in this study, both $M(t)$ and $R(t)$ are scalar quantities. The quantity $R(t)$ is defined as the covariance matrix of the measurement errors and is given by

$$R(t) = \sigma_T^2 = \sigma_I^2 + \frac{\sigma_H^2}{\left(r_{LM}^2 - r_p^2 \right)} \quad (A9)$$

When spacecraft-star measurements are processed, $\sigma_H = 0$ in this equation.

Finally, ΔQ is the difference between the value of the included angle actually measured and the expected value of the angle computed from the current estimate of the state vector.

APPENDIX B

SENSITIVITY VECTORS FOR SPACECRAFT-STAR AND SPACECRAFT-HORIZON MEASUREMENT TYPES

The sensitivity vector $\bar{H}(t)$, which relates measurement deviations to relative state deviations, is a function of the geometrical configuration of the celestial body (star or horizon) from which the measurement is made, and may be written

$$\bar{H}(t) = \nabla_{\bar{X}} Q_E(t) = \left[\bar{\alpha}^T \bar{\beta}^T \mathbf{1} \right] \quad (\text{B1})$$

where $\bar{\alpha}$ and $\bar{\beta}$ are six-dimensional column vectors defined as

$$\bar{\alpha} = \begin{bmatrix} \bar{\alpha}_1 \\ 0 \end{bmatrix}; \bar{\beta} = \begin{bmatrix} \bar{\beta}_1 \\ 0 \end{bmatrix} \quad (\text{B2})$$

For the spacecraft-star measurement $\bar{\alpha}_1$ is a null vector, and $\bar{\beta}_1$ can be written

$$\bar{\beta}_1 = \frac{\cos \Phi}{\rho_{cl} \sin \Phi} \bar{\rho}_{cl} - \frac{\bar{r}_s^o}{\rho_{cl} \sin \Phi} \quad (\text{B3})$$

For the spacecraft-horizon measurement $\bar{\alpha}_1$ is defined as

$$\bar{\alpha}_1 = \frac{\bar{\rho}_{cl}}{\sin(\beta + \gamma) \rho_{cl} r_{LM}} + \left[\frac{r_{moon}}{\cos \gamma r_{LM}^3} + \frac{\cos(\beta + \gamma)}{\sin(\beta + \gamma) r_{LM}^2} \right] \bar{r}_{LM} \quad (\text{B4})$$

and $\bar{\beta}_1$ is written

$$\bar{\beta}_1 = \left[\frac{1}{\sin(\beta + \gamma)\rho_{cl}r_{LM}} - \frac{r_{moon}}{\cos \gamma r_{LM}^3} - \frac{\cos(\beta + \gamma)}{\sin(\beta + \gamma)r_{LM}^2} \right] \bar{r}_{LM} + \left[\frac{\cos(\beta + \gamma)}{\sin(\beta + \gamma)\rho_{cl}^2} - \frac{1}{\sin(\beta + \gamma)\rho_{cl}r_{LM}} \right] \bar{\rho}_{cl} \quad (B5)$$

It should be noted that the angles ϕ and β appearing in these equations are restricted to values $\leq 50^\circ$ according to the field-of-view constraint outlined in the assumptions section of the text.

APPENDIX C

NUMERICAL OPTIMIZATION TECHNIQUE

FOR STAR SELECTION

When selecting stars on the basis of minimizing the total rms relative position uncertainty at the measurement time, the following procedure was used.

Equation (A5) can be rewritten

$$\hat{W}^*(t_M) = \hat{W}(t_M) - \Delta\hat{W}_i(t_M) \quad (C1)$$

where $\Delta\hat{W}_i(t_M)$ represents the change in $\hat{W}(t_M)$ as a result of processing the measurement at the measurement time t_M . At each t_M , $\Delta\hat{W}_i$ is computed for each of the 20 stars ($i = 1, 2, \dots, 20$), and the $\Delta\hat{W}_i$ which produces the maximum reduction in total relative position error selects the star to be used.

The selection of stars nearest the measurement plane involved a simpler procedure. Using the equation

$$\left| \bar{r}_{s,i}^0 \cdot \bar{r}_{LM}(t_M) \times \bar{r}_{CSM}(t_M) \right| = \left| P_i(t_M) \right| \quad (C2)$$

at each measurement time, that star is selected which produces the minimum $|P_i|$.

REFERENCES

1. U. S. Air Force Operating Manual: Hand-Held Space Sextant. Prepared by Kollsman Instrument Corporation, Space Div. , for Air Force Avionics Laboratory (RTD), Wright-Patterson Air Force Base. Contract No. AF33(615)3088, Project No. 4200, Task No. 420019, Oct. 1965.
2. Battin, R. H. : Astronautical Guidance. McGraw-Hill Book Co. , Inc. (New York, N. Y.), 1964, chapter 9.
3. MIT/IL Report No. R-547: PGNC System Operations Plan Mission AS-207/8. MIT Instrumentation Laboratory (Cambridge, Mass.), Oct. 1966.

TABLE I. - ABBREVIATED 20-STAR CATALOGUE USED
WITH DIGITAL COMPUTER SIMULATION

Star name	Magnitude	Right ascension, deg	Declination, deg
α Andromedae	2.1	1.45	28.81
α Eradani (Achernar)	0.6	23.97	-57.49
α Tauri (Aldebaran)	1.1	68.26	16.40
α Aurigae	0.2	78.25	45.94
α Orionis	0.9	88.12	7.39
α Carinae	-0.9	95.71	-52.66
α Canis Majoris (Sirius)	-1.6	100.73	-16.65
α Canis Minoris (Procyon)	0.5	114.17	5.35
β Geminorum (Pollux)	1.2	115.56	28.14
β Carinae	1.8	138.17	-69.50
α Leonis (Regulus)	1.3	151.42	12.21
η Ursae Majoris	1.9	-153.61	49.55
α Bootis (Arcturus)	0.2	-146.66	19.43
α Centauri	0.1	-140.98	-60.62
α Scorpii (Antares)	1.2	-113.42	-26.32
α Lyrae (Vega)	0.1	-81.19	38.73
α Aquilae	0.9	-62.91	8.73
α Cygni (Deneb)	1.3	-50.07	45.10
α Piscis Austrini (Fomalhaut)	1.3	-16.27	-29.89
α Ursae Minoris (Polaris)	2.1	27.31	89.03

TABLE II. - COMPARISON OF UNCERTAINTIES AT RENDEZVOUS - SPACECRAFT-HORIZON
MEASUREMENTS PROCESSED AFTER CIRCULARIZATION AND NOT PROCESSED
AFTER CIRCULARIZATION

Case number	Sensor spacecraft-horizon measurements processed after circularization						Sensor spacecraft-horizon measurements not processed after circularization					
	Root-mean-square relative altitude error, n. mi.	Root-mean-square relative range error, n. mi.	Root-mean-square relative track error, n. mi.	Root-mean-square relative altitude rate error, fps	Root-mean-square relative range rate error, fps	Root-mean-square relative track rate error, fps	Root-mean-square relative altitude error, n. mi.	Root-mean-square relative range error, n. mi.	Root-mean-square relative range error, n. mi.	Root-mean-square relative altitude rate error, fps	Root-mean-square relative range rate error, fps	Root-mean-square relative track rate error, fps
^a I	0.06	0.25	0.01	1.35	0.20	0.06	0.13	0.66	0.01	3.45	0.45	0.06
^b II	0.08	0.32	0.01	1.70	0.31	0.07	0.18	0.94	0.01	4.81	0.62	0.07
^c III	0.06	0.25	0.01	1.36	0.20	0.08	0.14	0.70	0.01	3.64	0.48	0.08
^d IV	0.07	0.31	0.01	1.65	0.25	0.09	0.17	0.89	0.01	4.57	0.60	0.09

^aMeasurements processed at 2-minute intervals, selecting stars to minimize total relative rms position at each measurement up to circularization.

^bSame as in case I, with measurements processed at 6-minute intervals.

^cMeasurements processed at 2-minute intervals, selecting stars nearest measurement plane up to circularization.

^dSame as in case III, with measurements processed at 6-minute intervals.

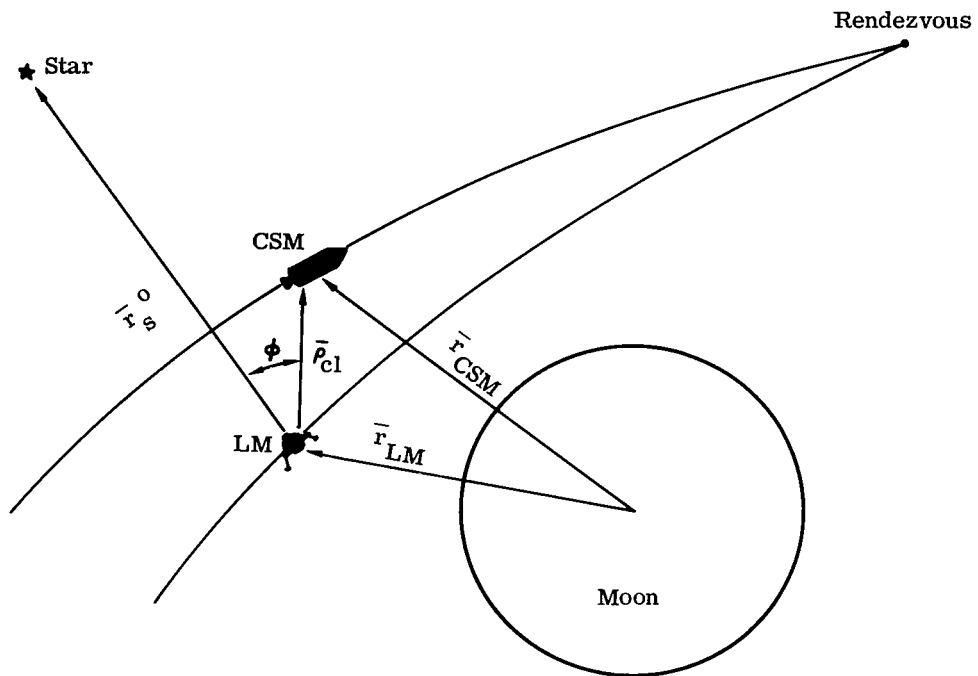


Figure 1. - Geometry of spacecraft-star included angle measurement.

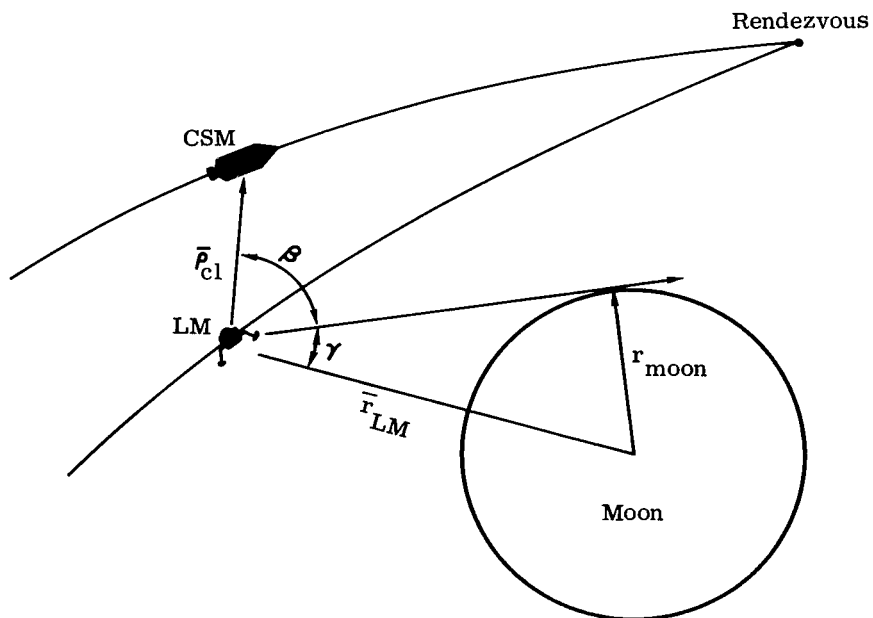
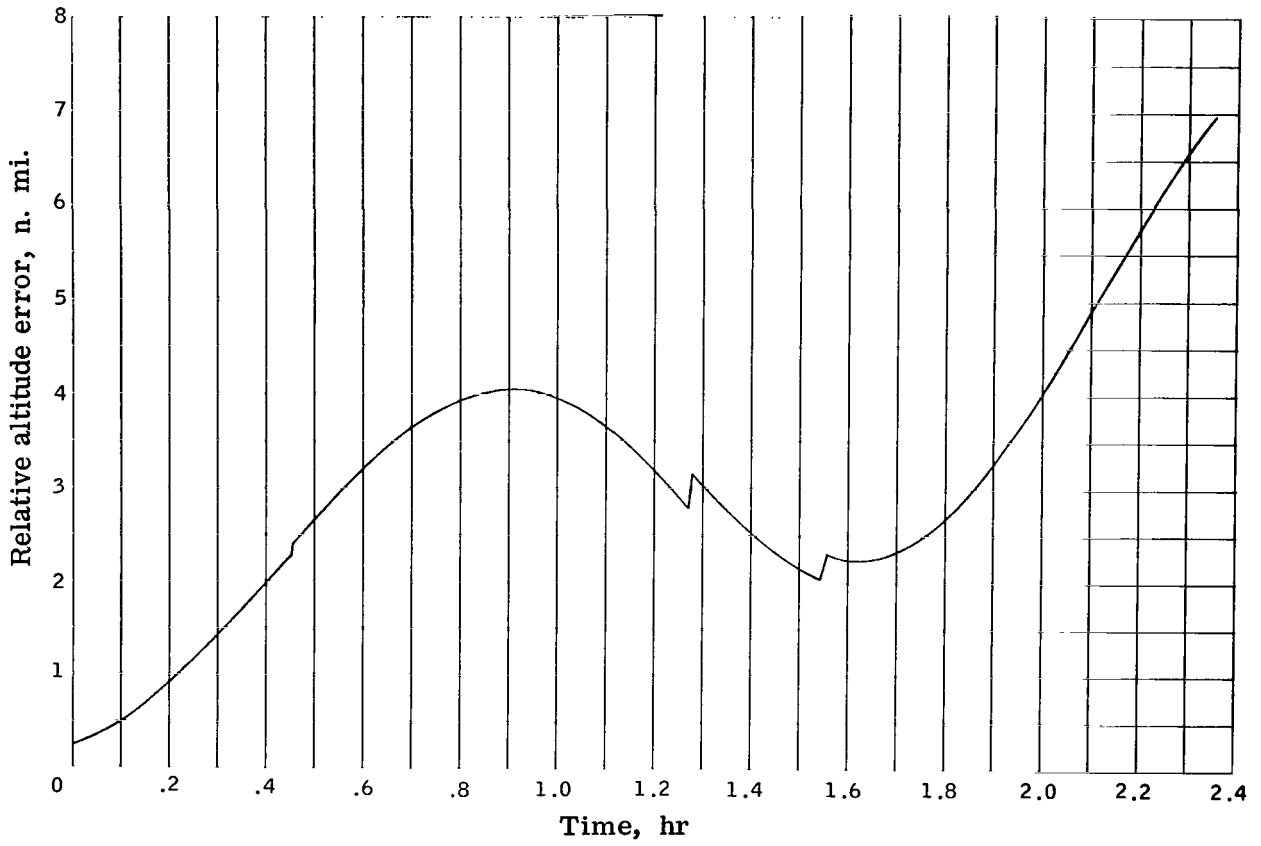
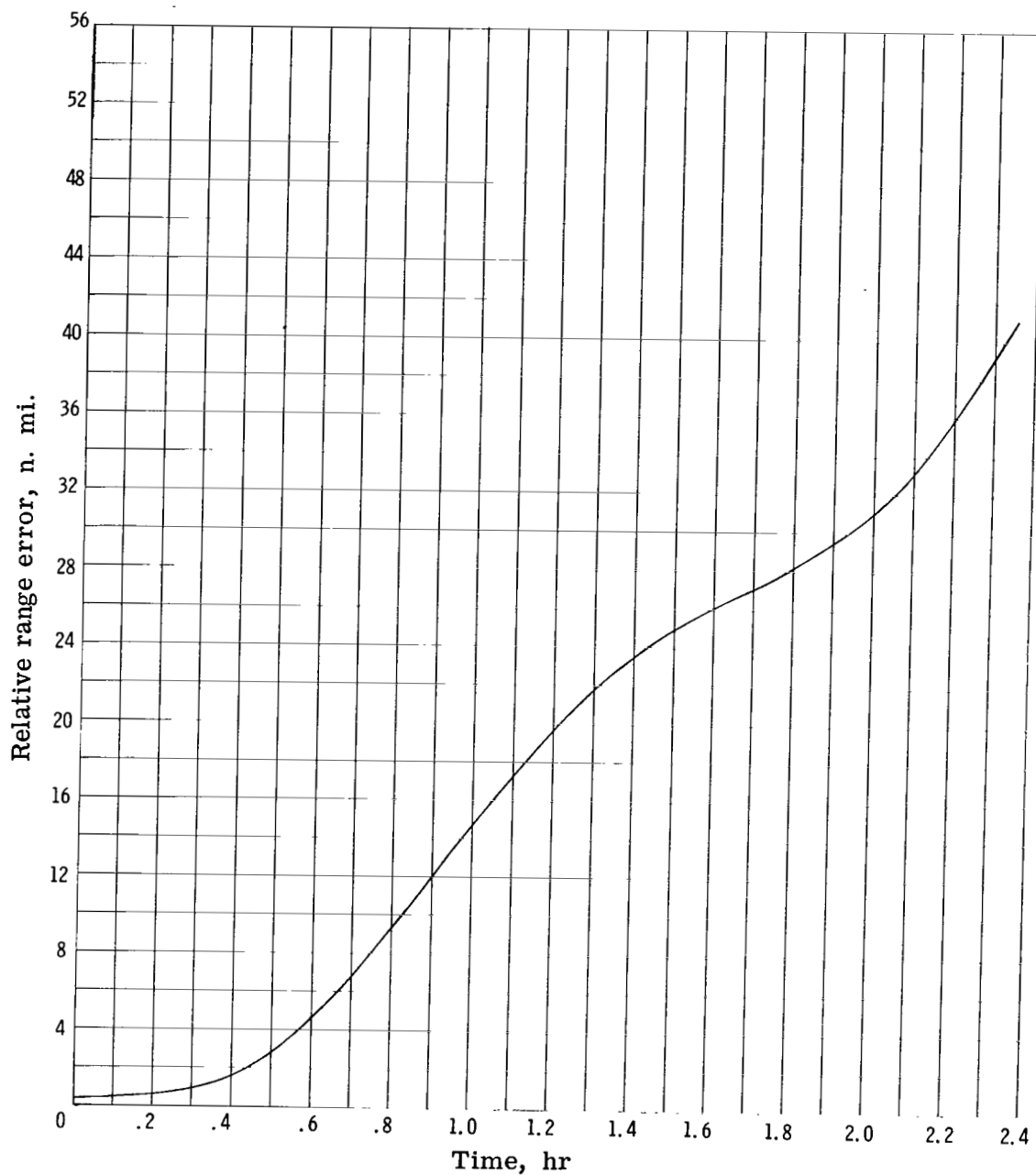


Figure 2. - Geometry of spacecraft-lunar horizon included angle measurement.



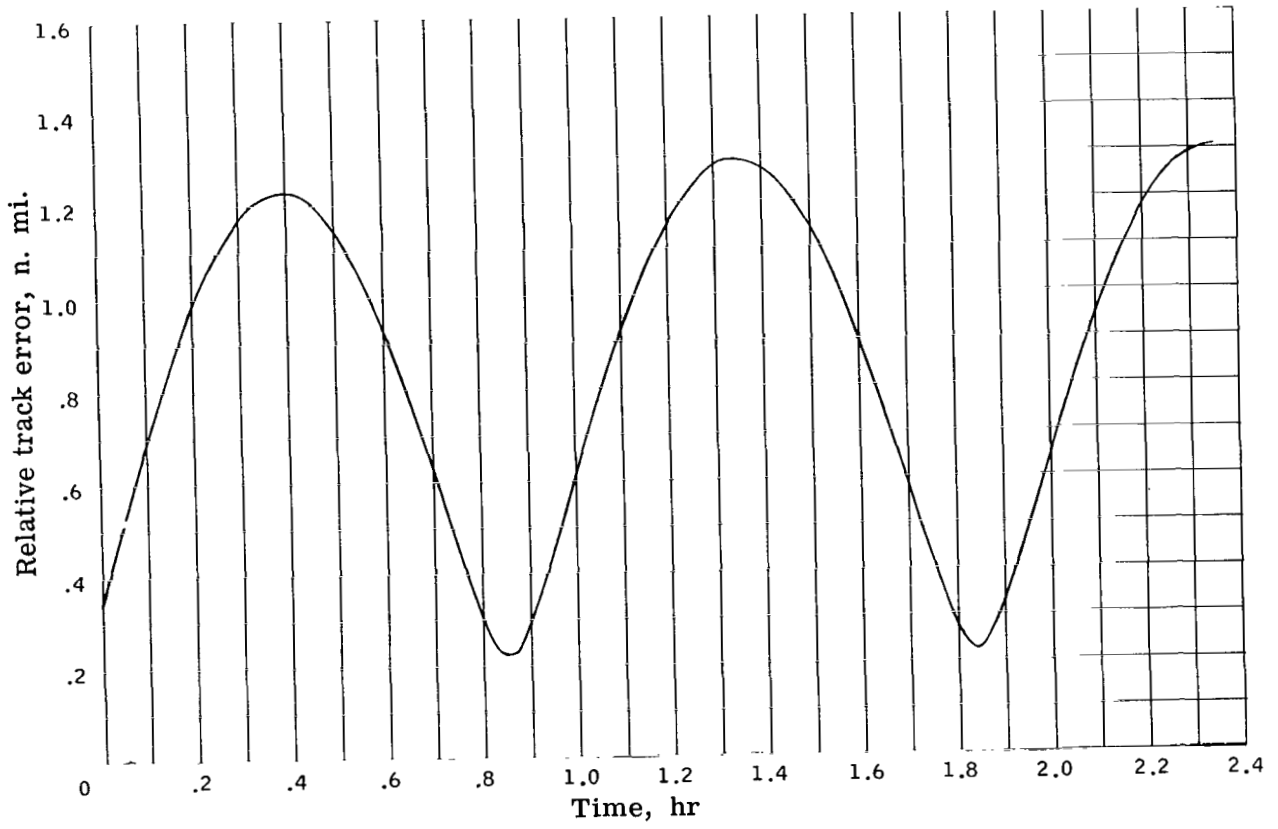
(a) Relative altitude error.

Figure 4. - No measurements processed from burnout to rendezvous.



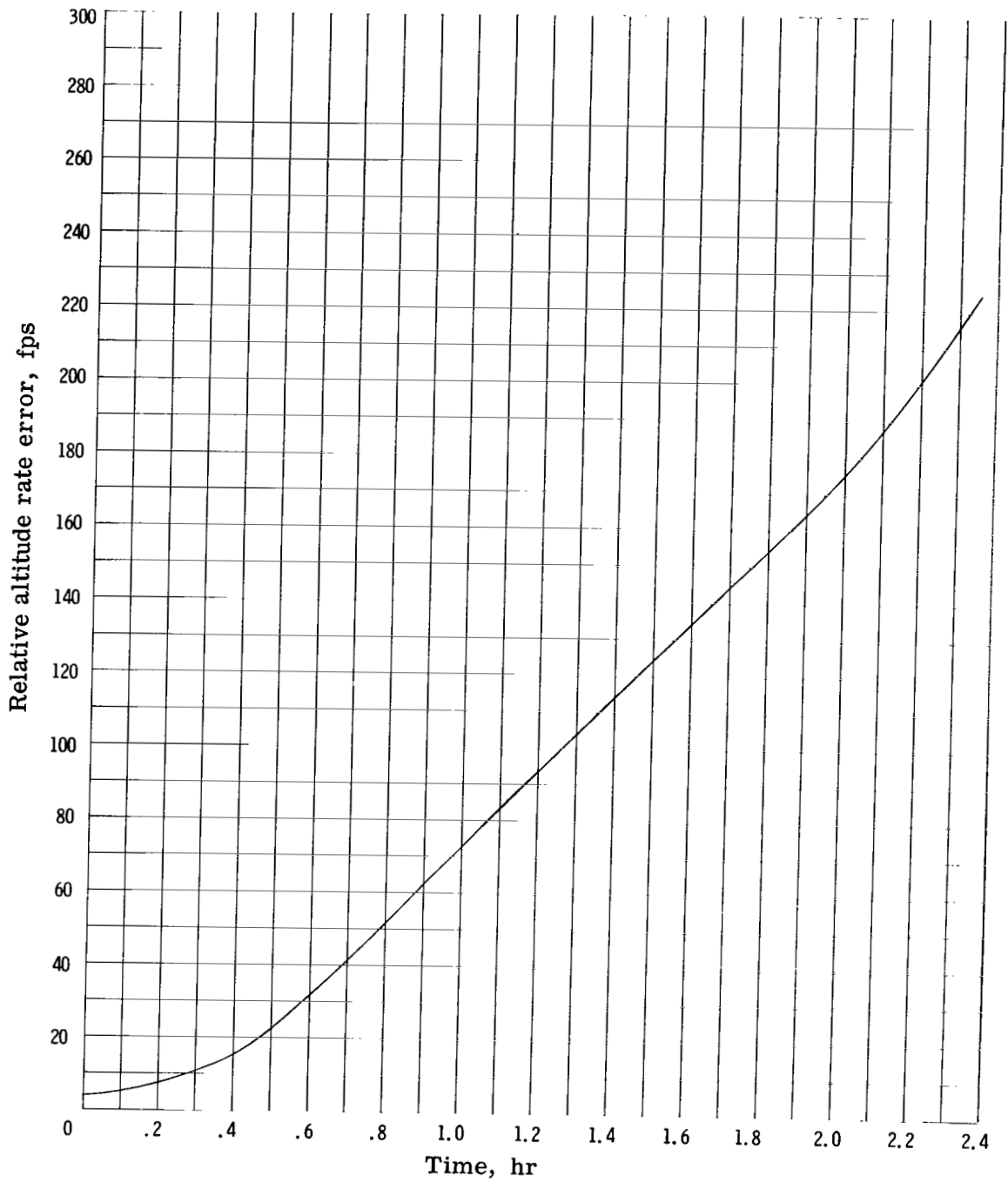
(b) Relative range error.

Figure 4. - Continued.



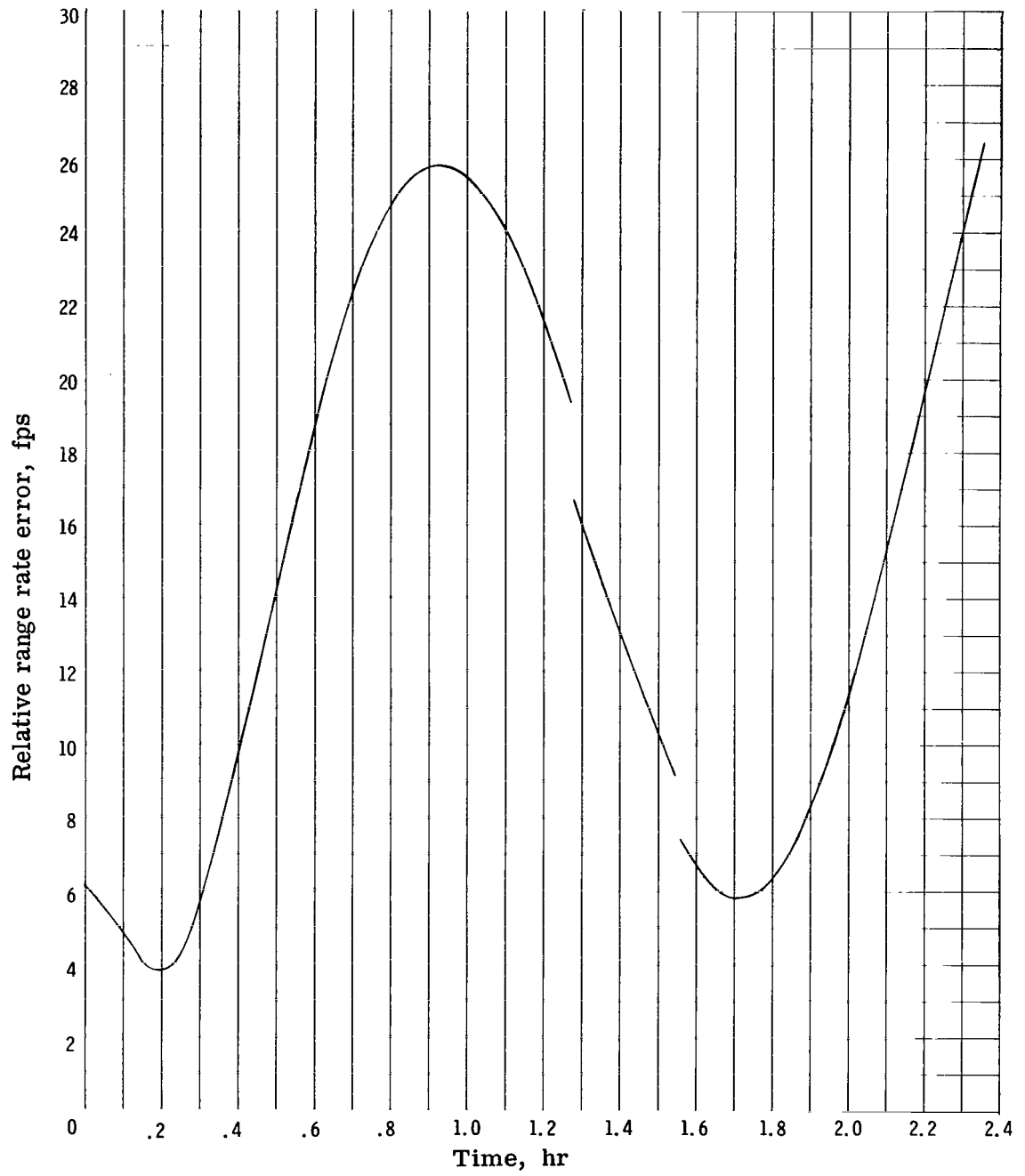
(c) Relative track error.

Figure 4. - Concluded.



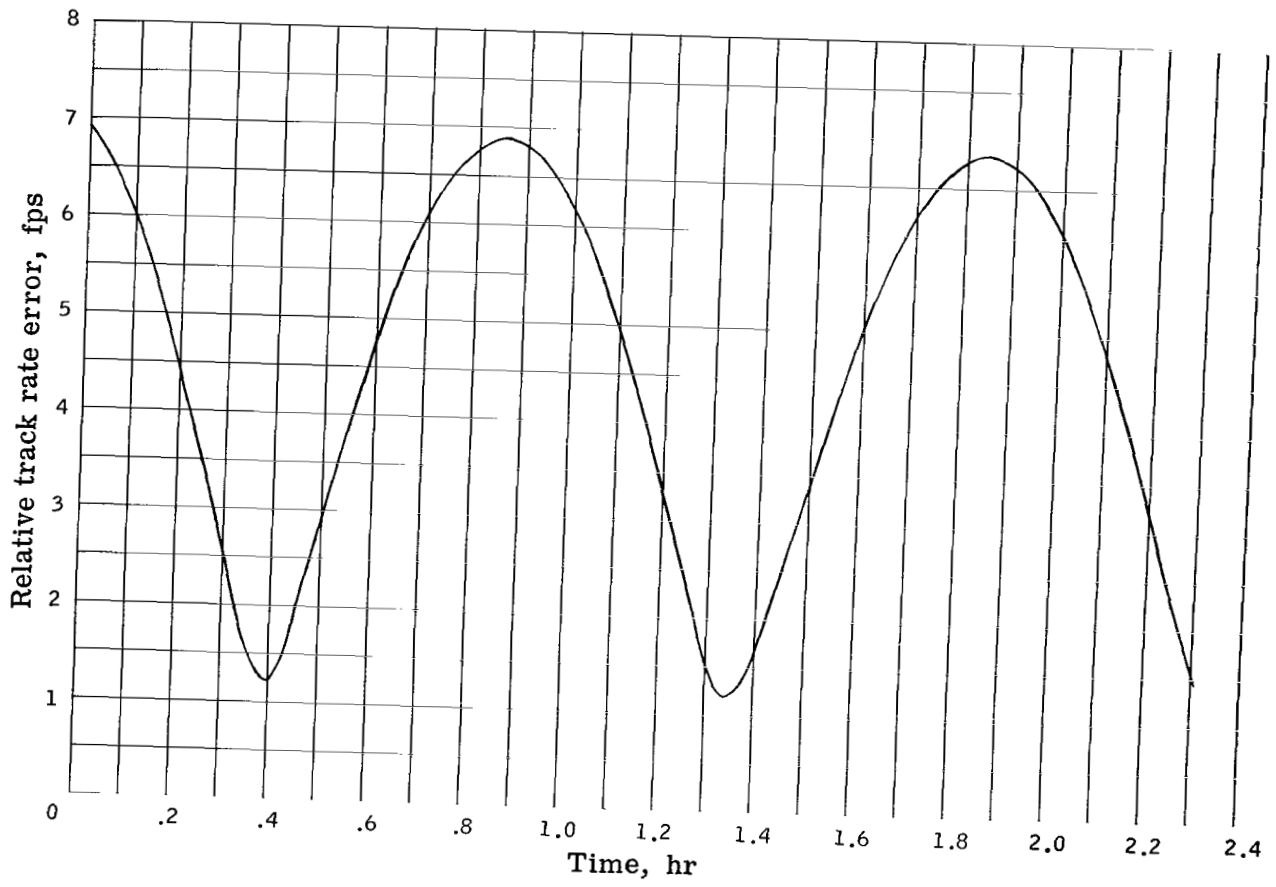
(a) Relative altitude rate error.

Figure 5. - No measurements processed from burnout to rendezvous.



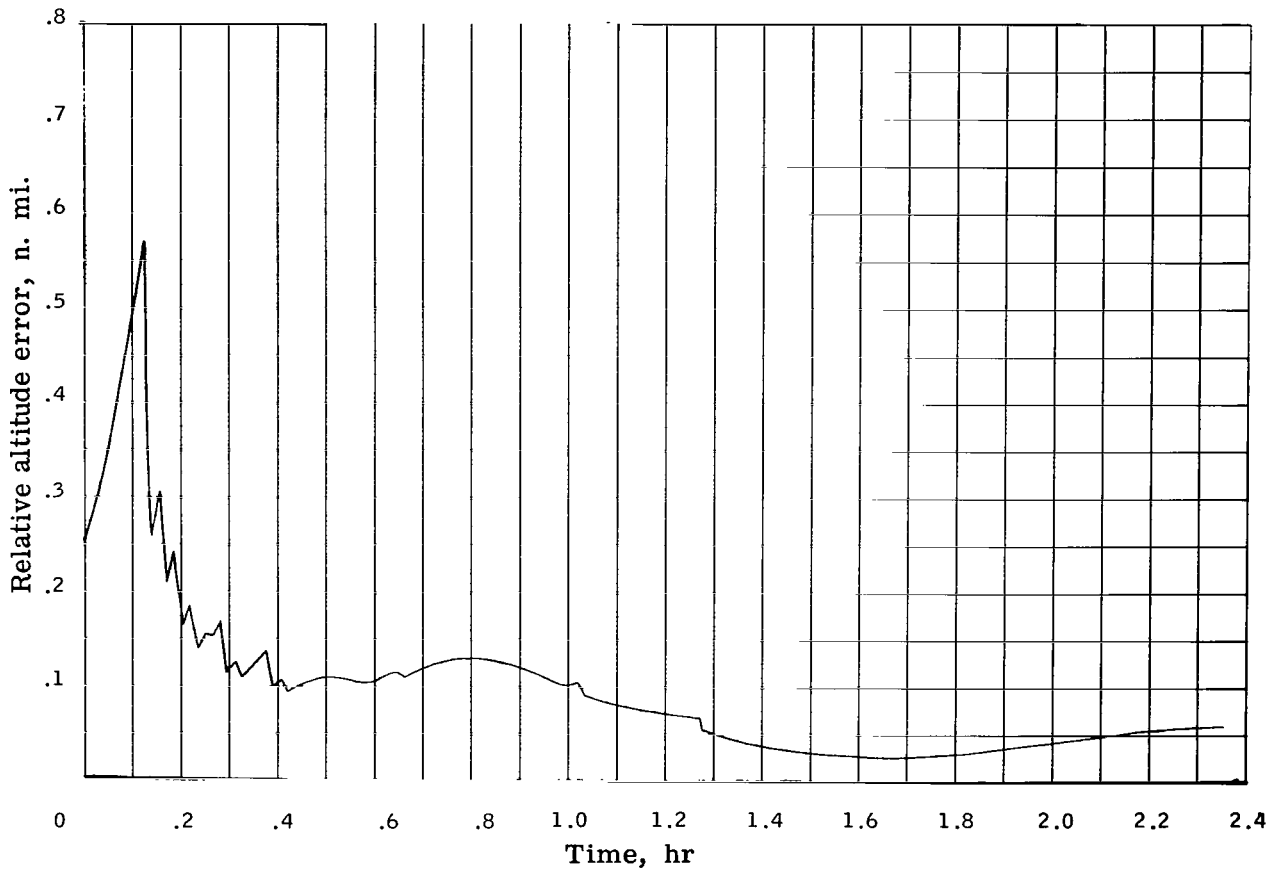
(b) Relative range rate error.

Figure 5. - Continued.



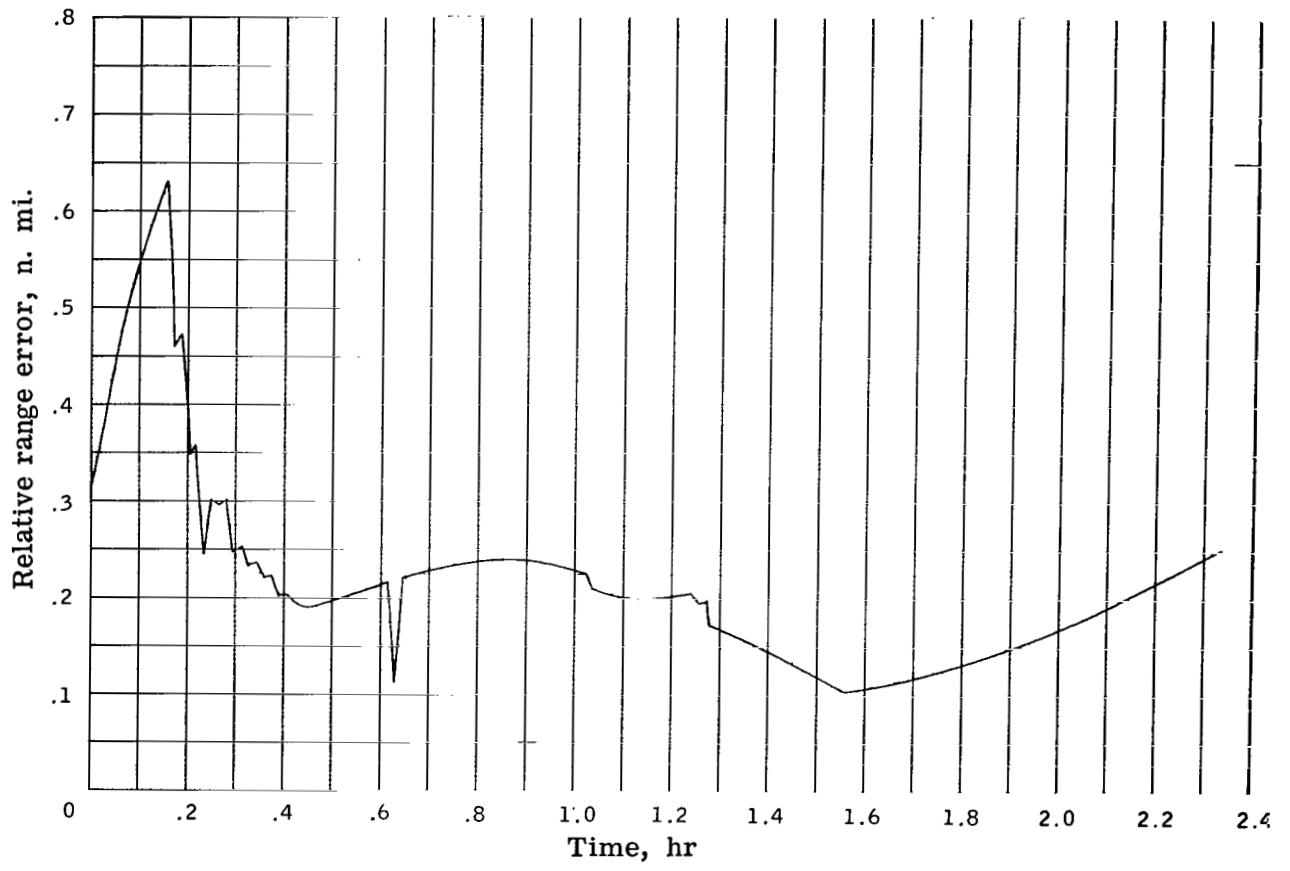
(c) Relative track rate error.

Figure 5. - Concluded.



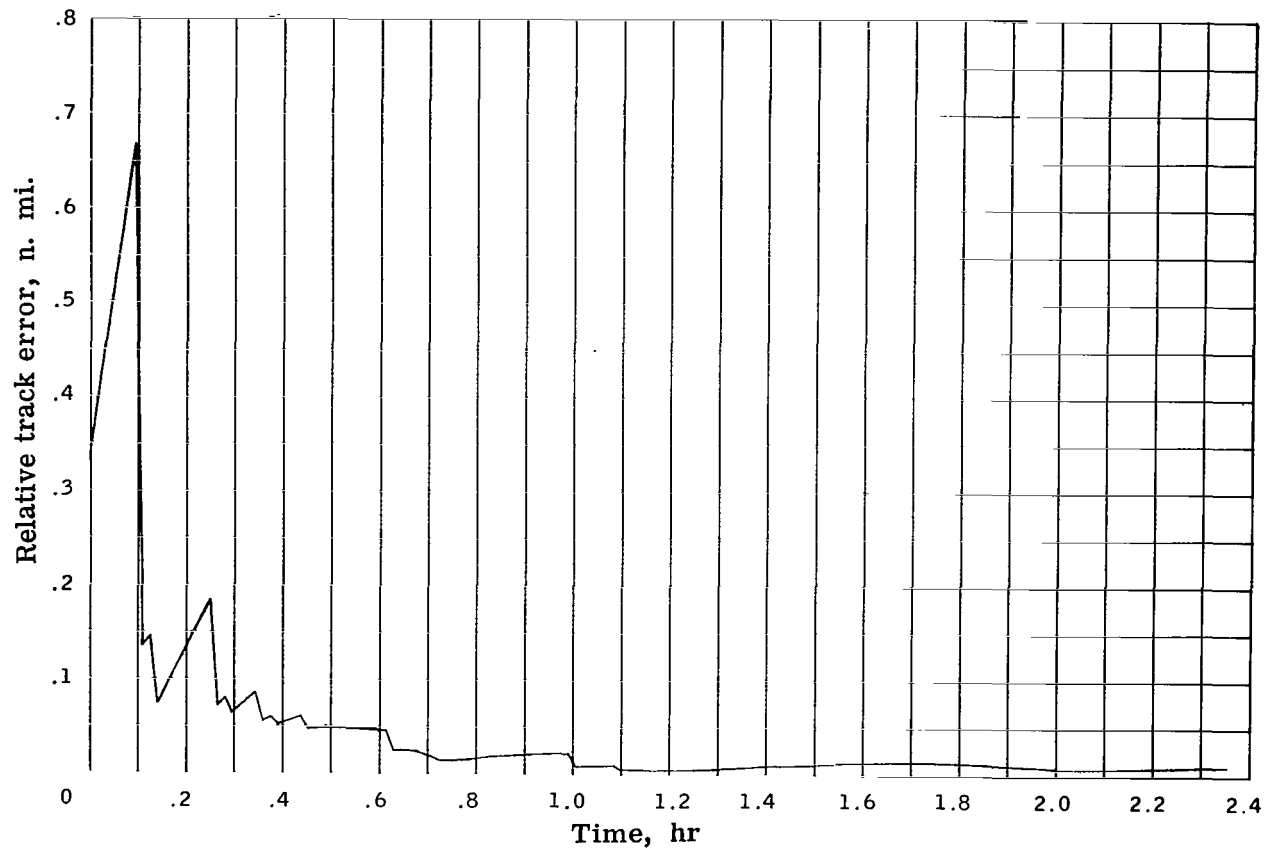
(a) Relative altitude error.

Figure 6. - Spacecraft-star measurements choosing stars to minimize total relative rms position processed every 2 minutes up to circularization; spacecraft-lunar horizon measurements processed thereafter.



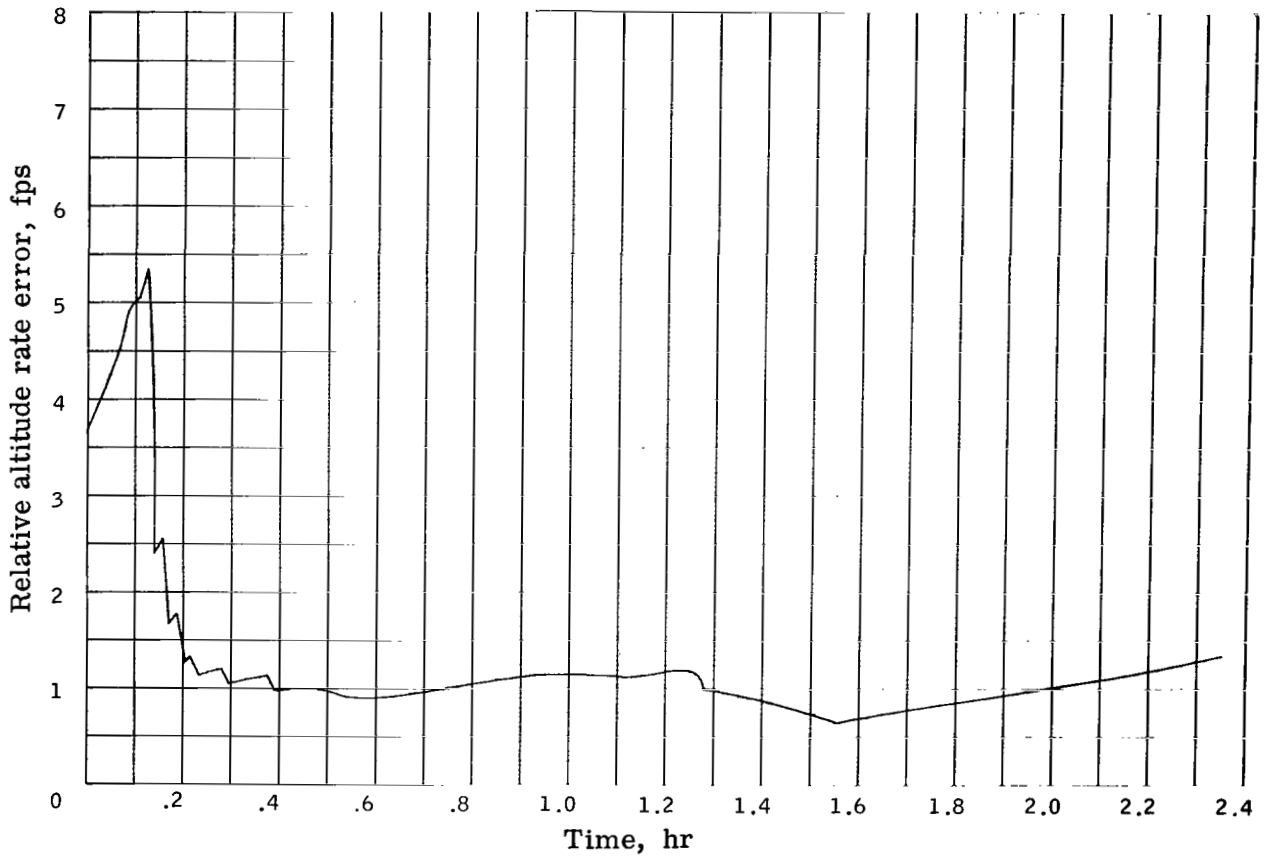
(b) Relative range error.

Figure 6.- Continued.



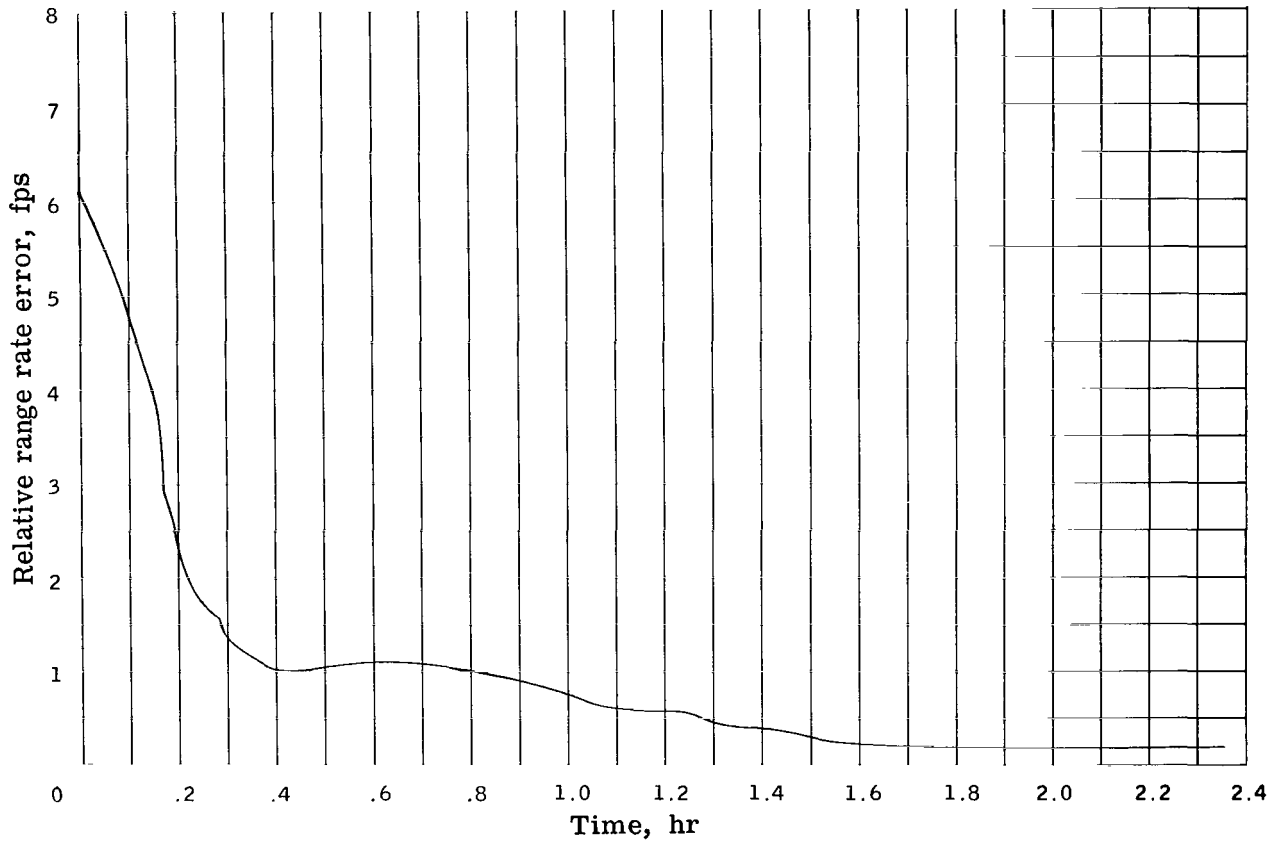
(c) Relative track error.

Figure 6.- Concluded.



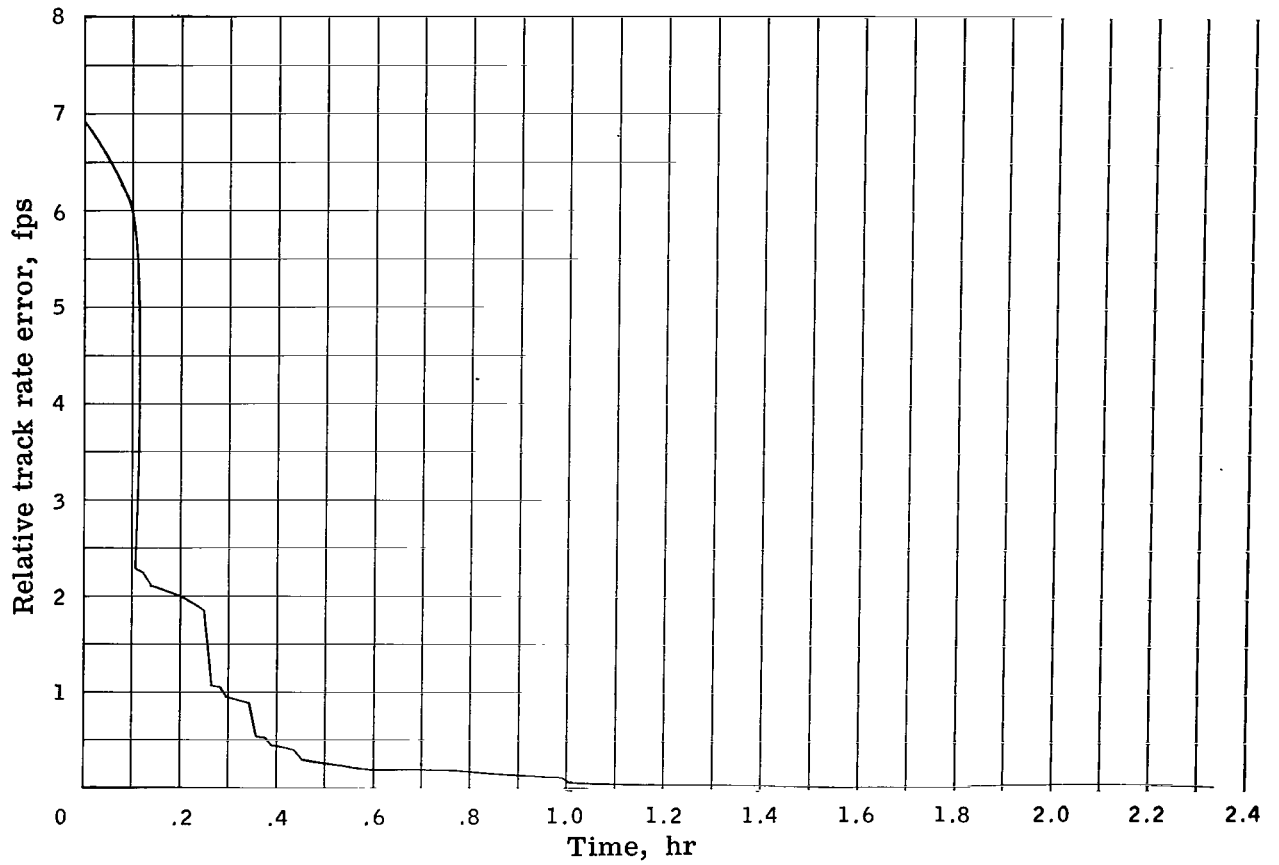
(a) Relative altitude rate error.

Figure 7. - Spacecraft-star measurements choosing stars to minimize total relative rms position processed every 2 minutes up to circularization; spacecraft-lunar horizon measurements processed thereafter.



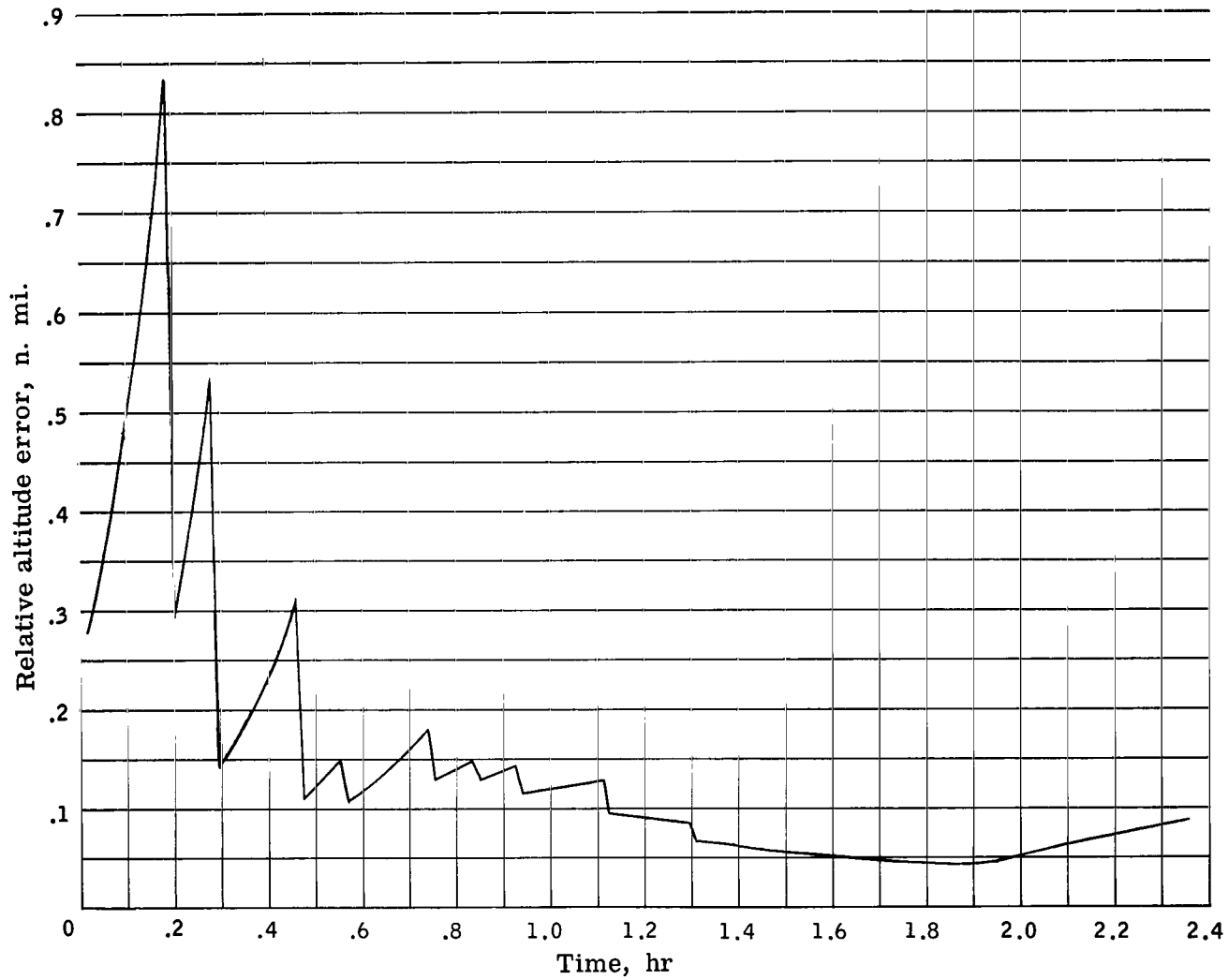
(b) Relative range rate error.

Figure 7. - Continued.



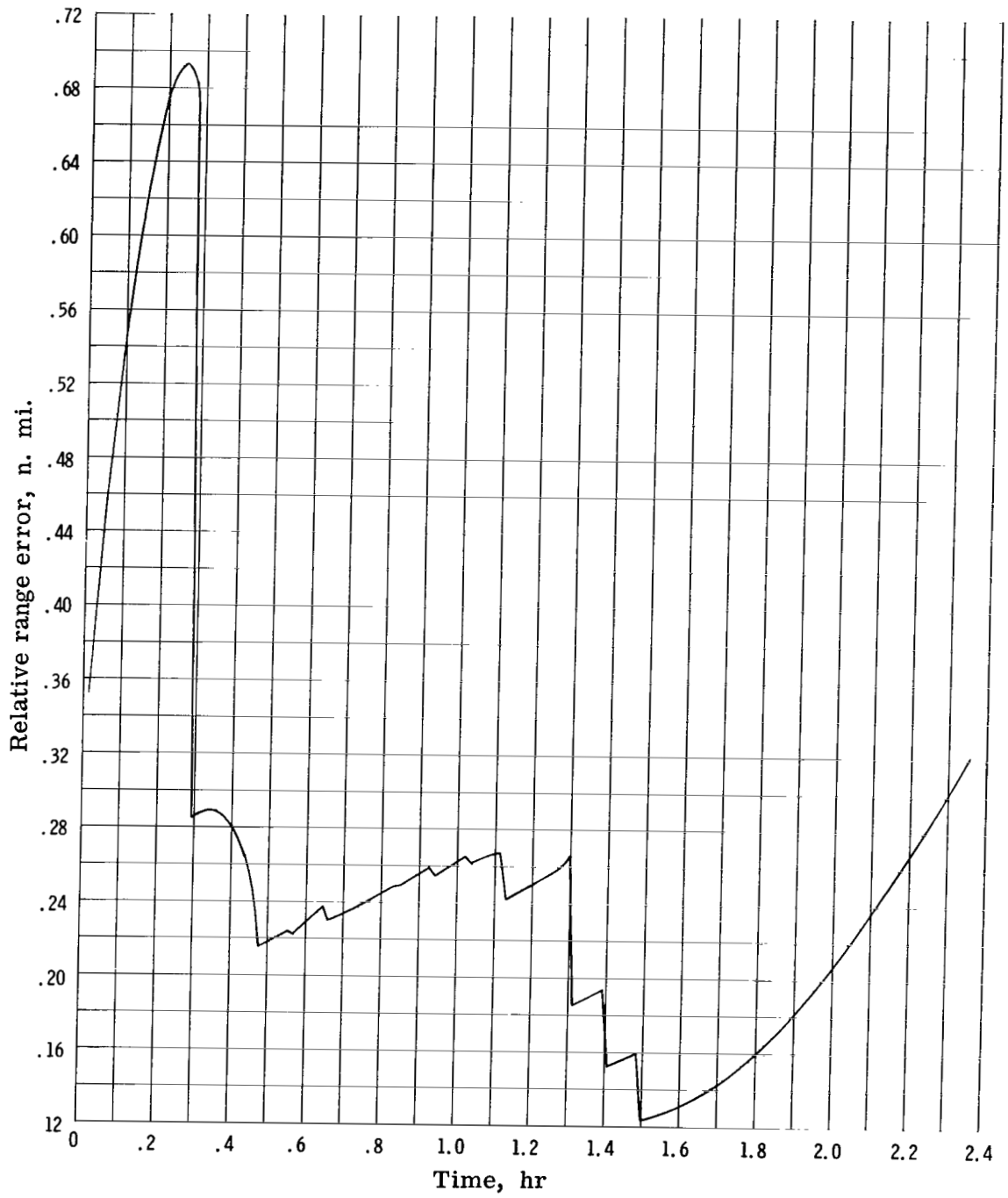
(c) Relative track rate error.

Figure 7.- Concluded.



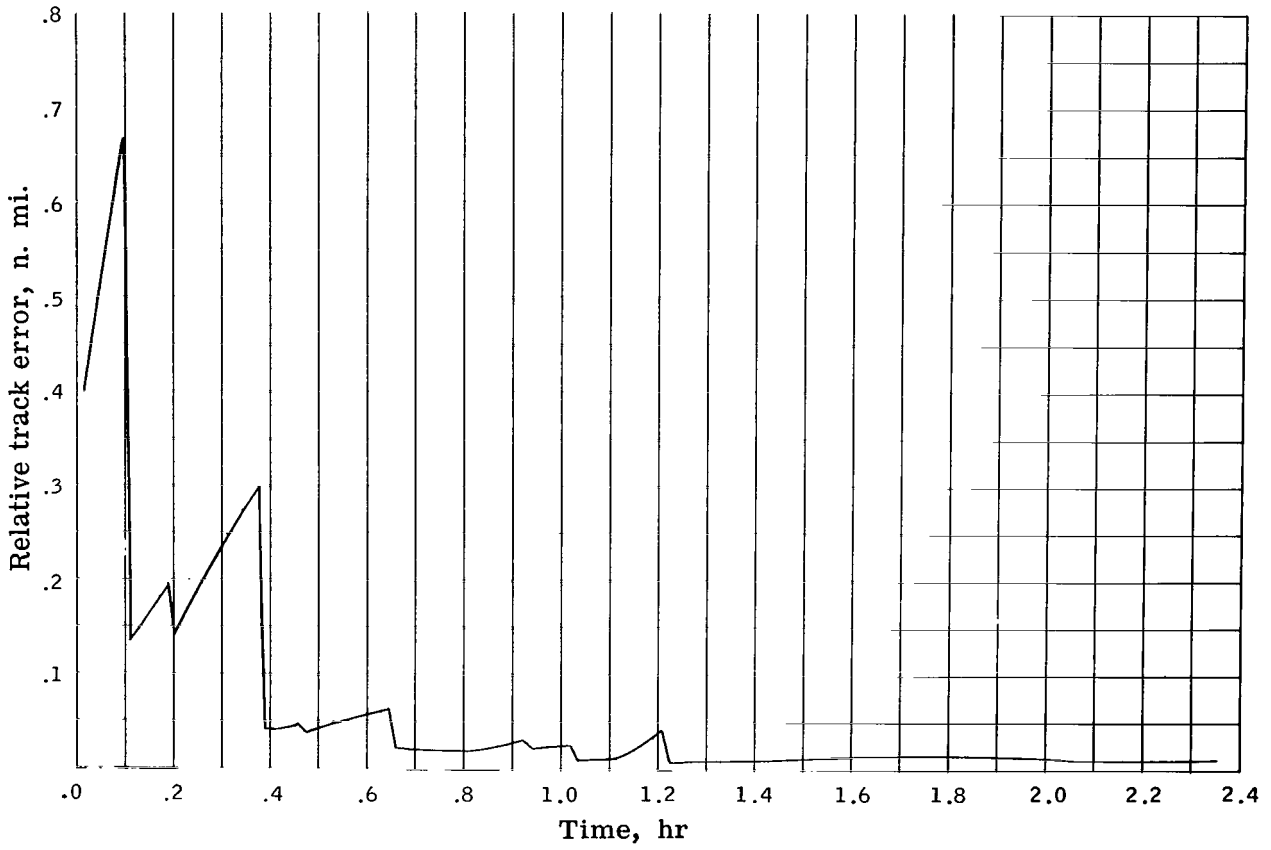
(a) Relative altitude error.

Figure 8.- Spacecraft-star measurements choosing stars to minimize total relative rms position processed every 6 minutes up to circularization; spacecraft-lunar horizon measurements processed thereafter.



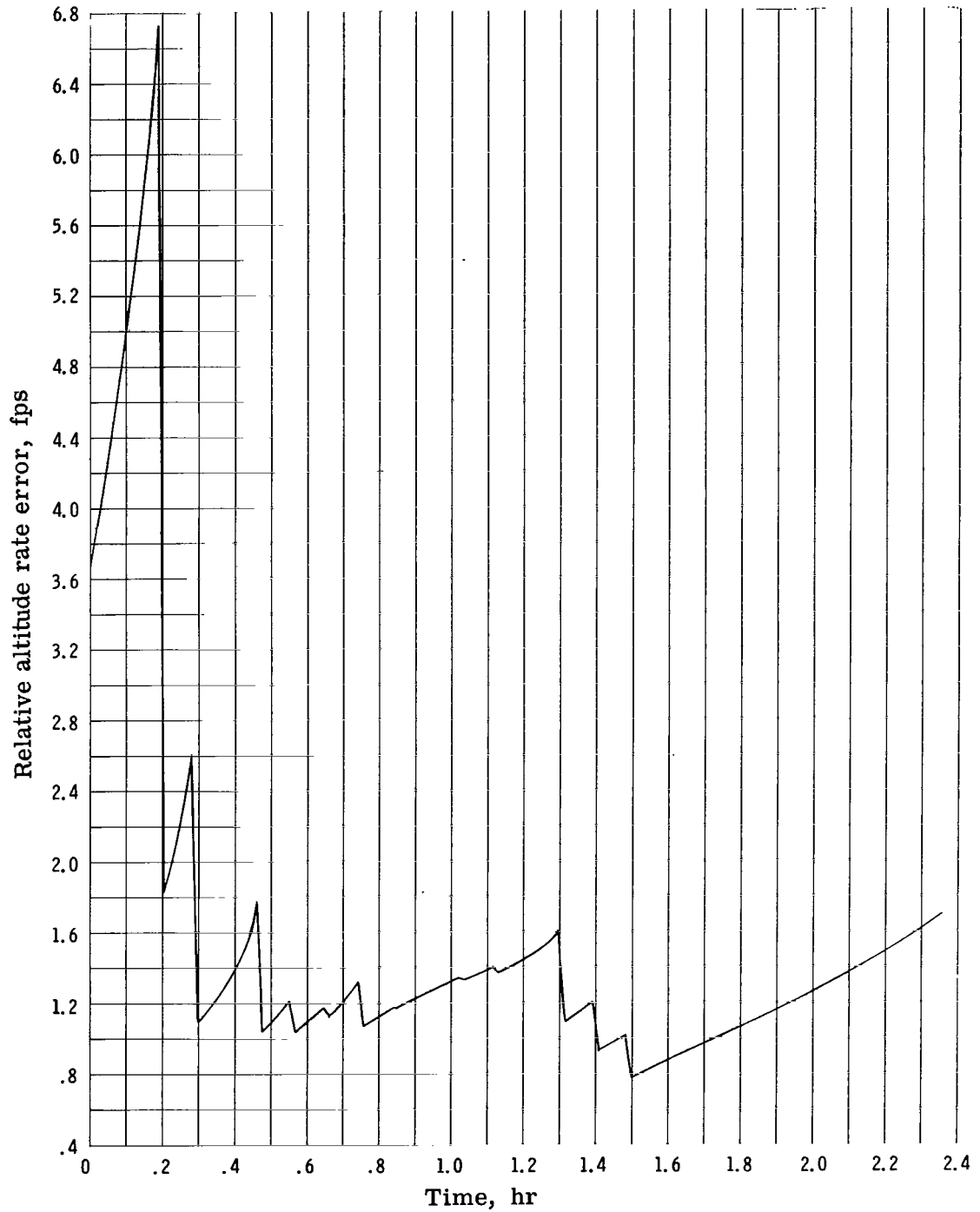
(b) Relative range error.

Figure 8. - Continued.



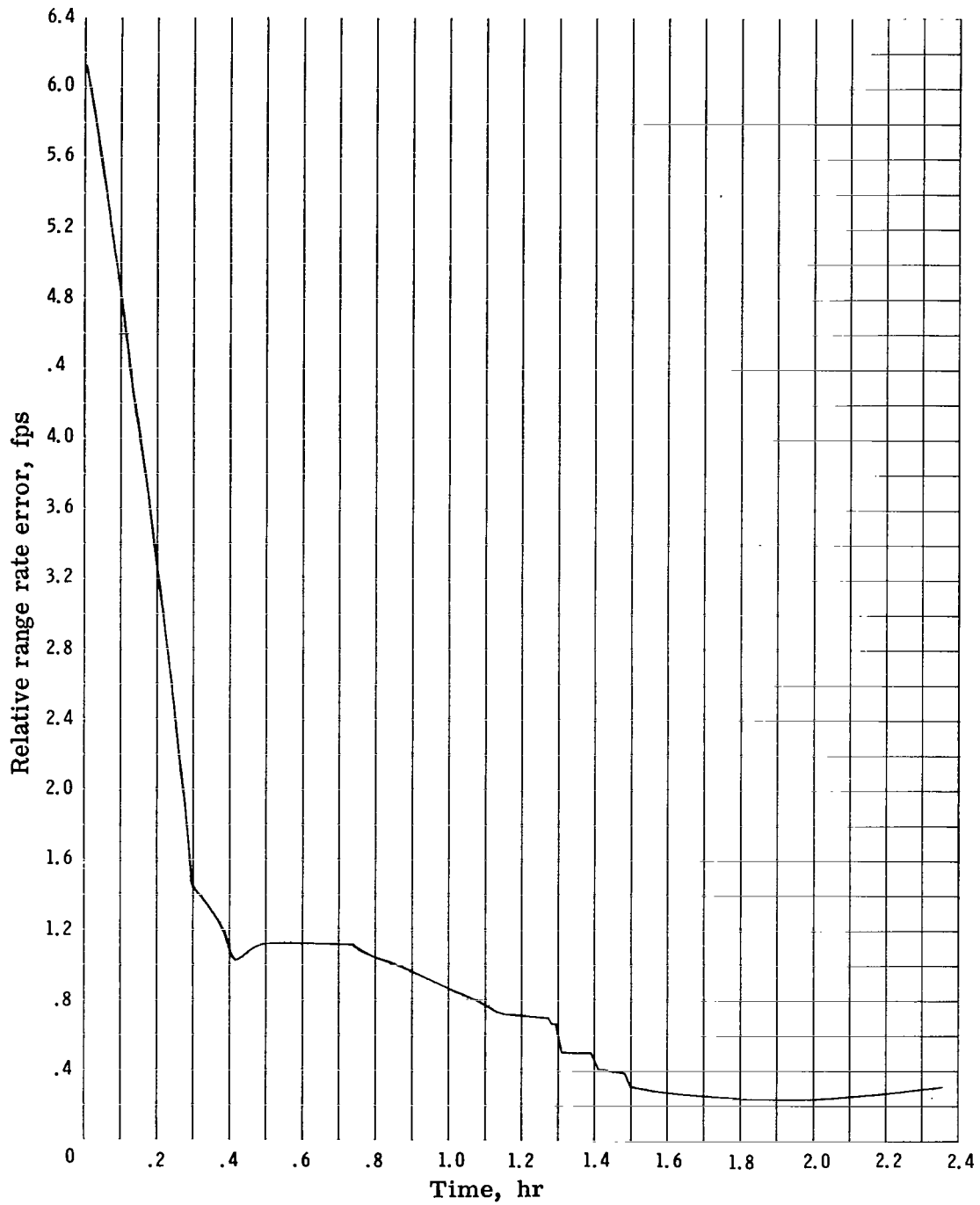
(c) Relative track error.

Figure 8. - Concluded.



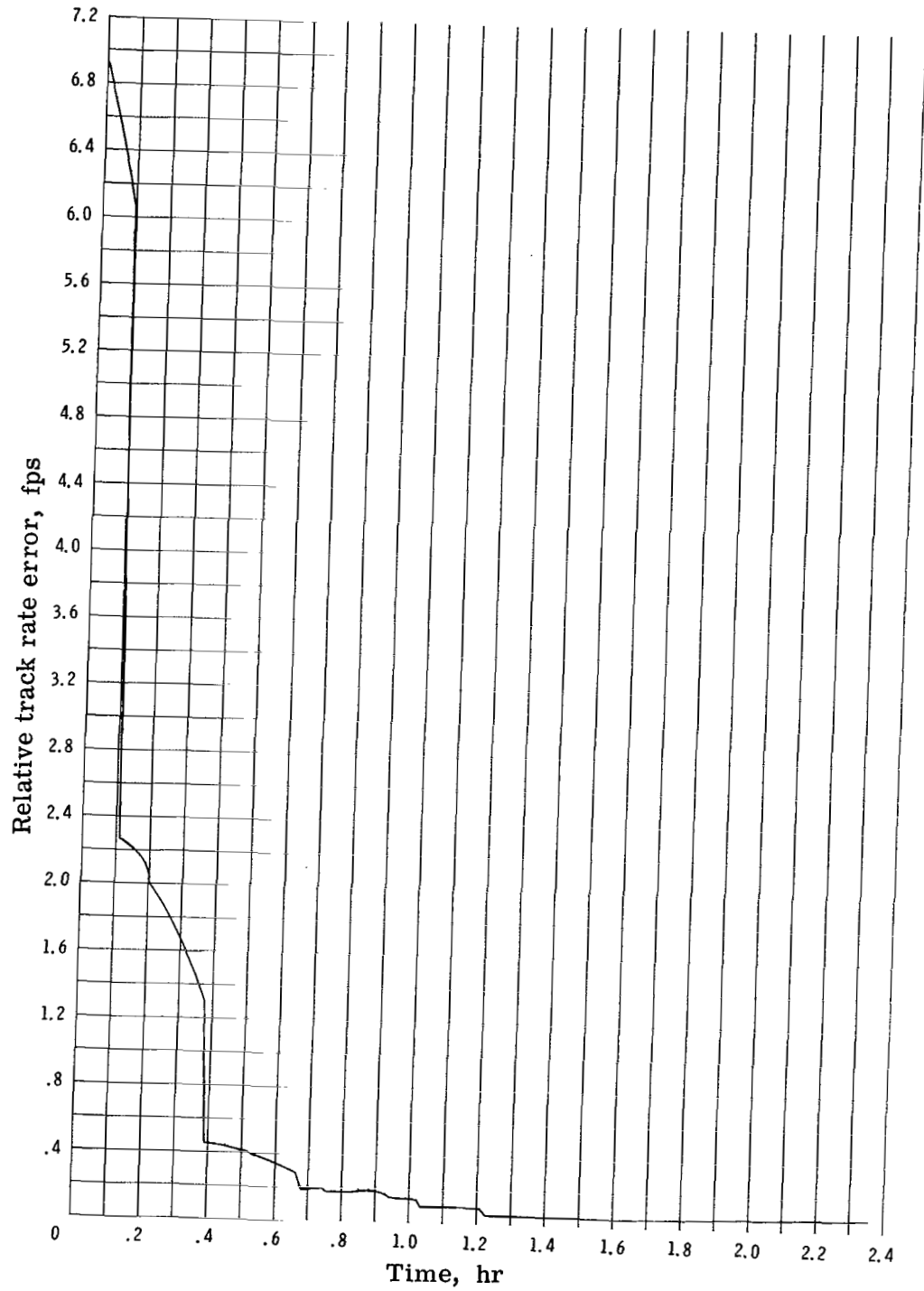
(a) Relative altitude rate error.

Figure 9. - Spacecraft-star measurements choosing stars to minimize total relative rms position processed every 6 minutes up to circularization; spacecraft-lunar horizon measurements processed thereafter.



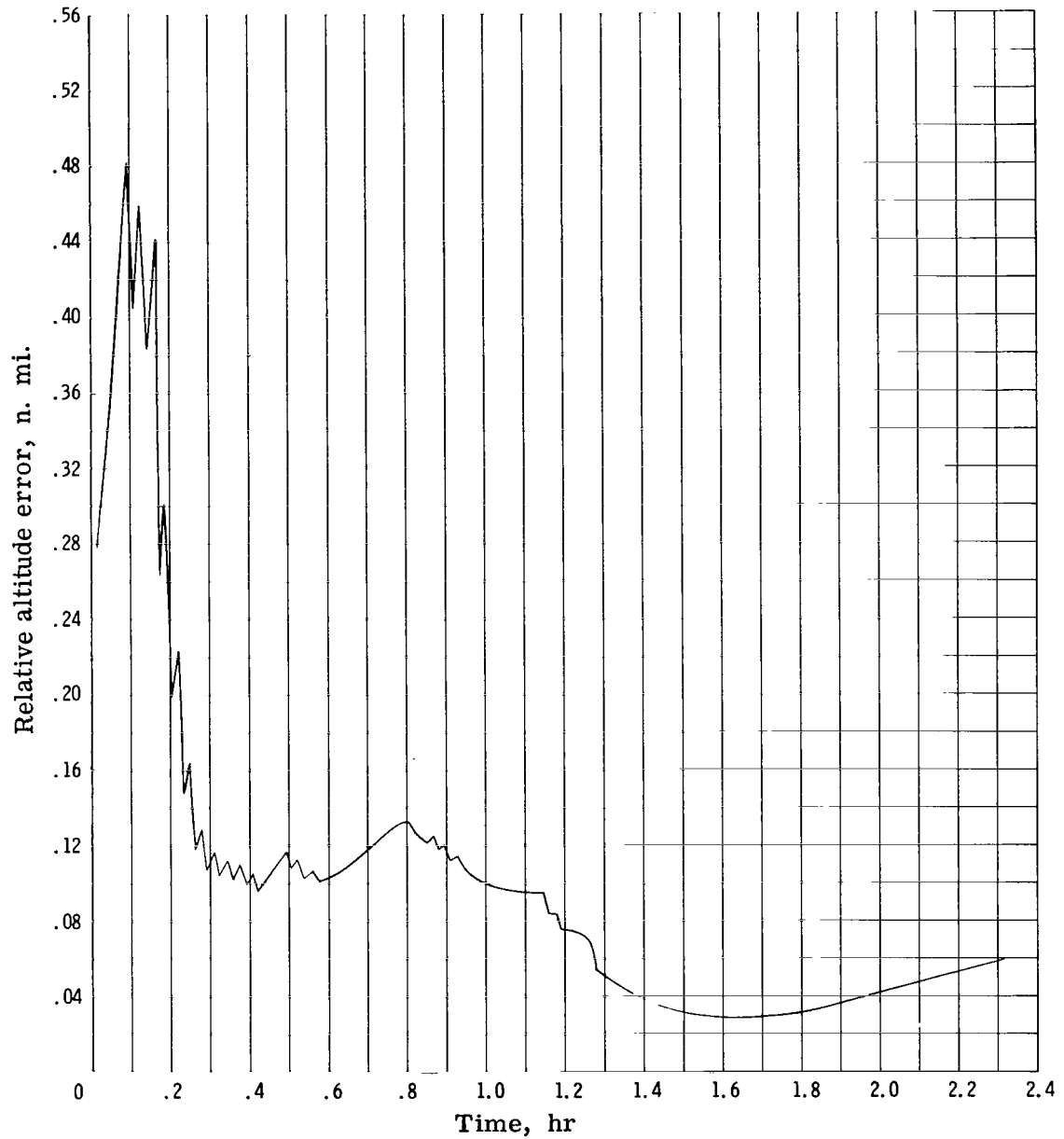
(b) Relative range rate error.

Figure 9. - Continued.



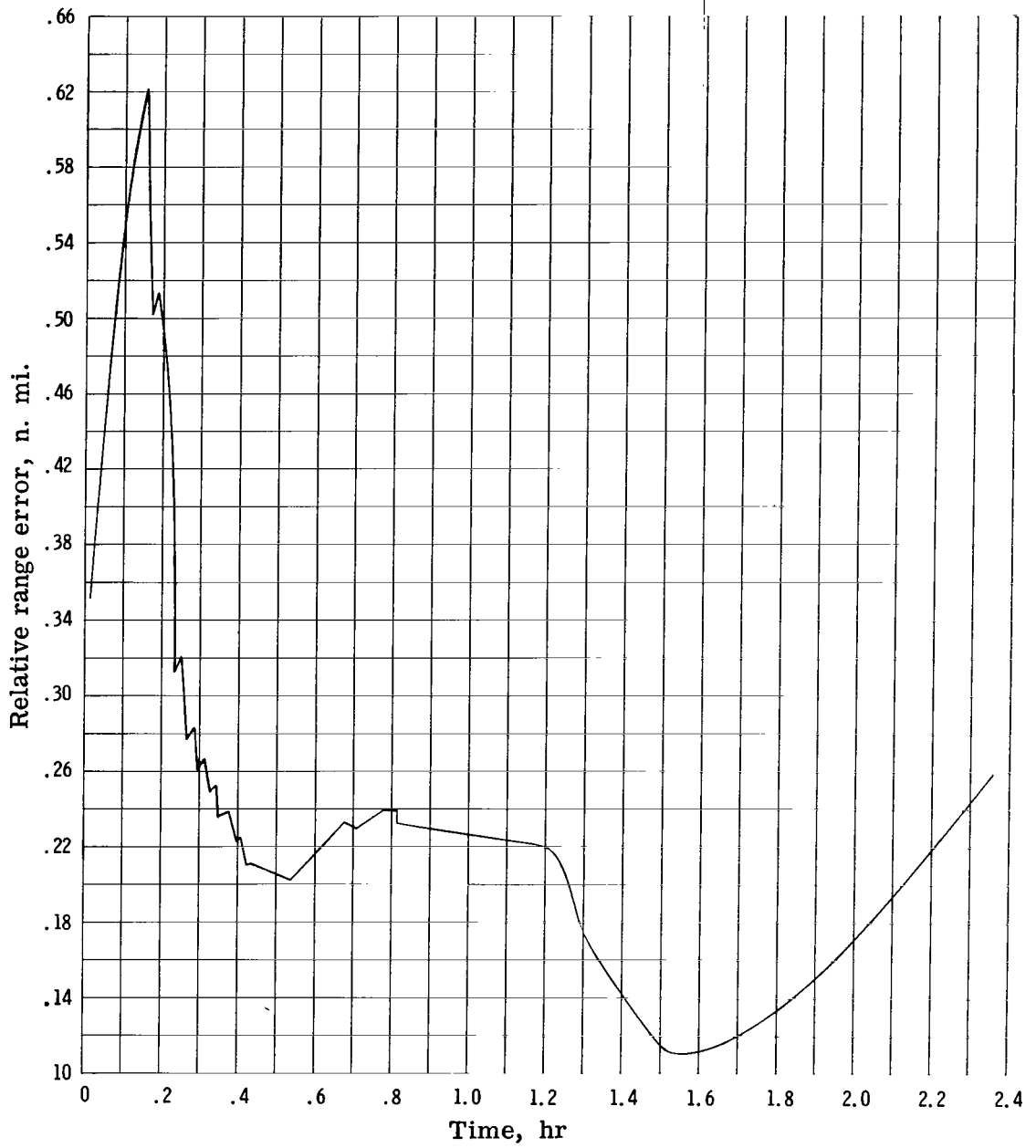
(c) Relative track rate error.

Figure 9. - Concluded.



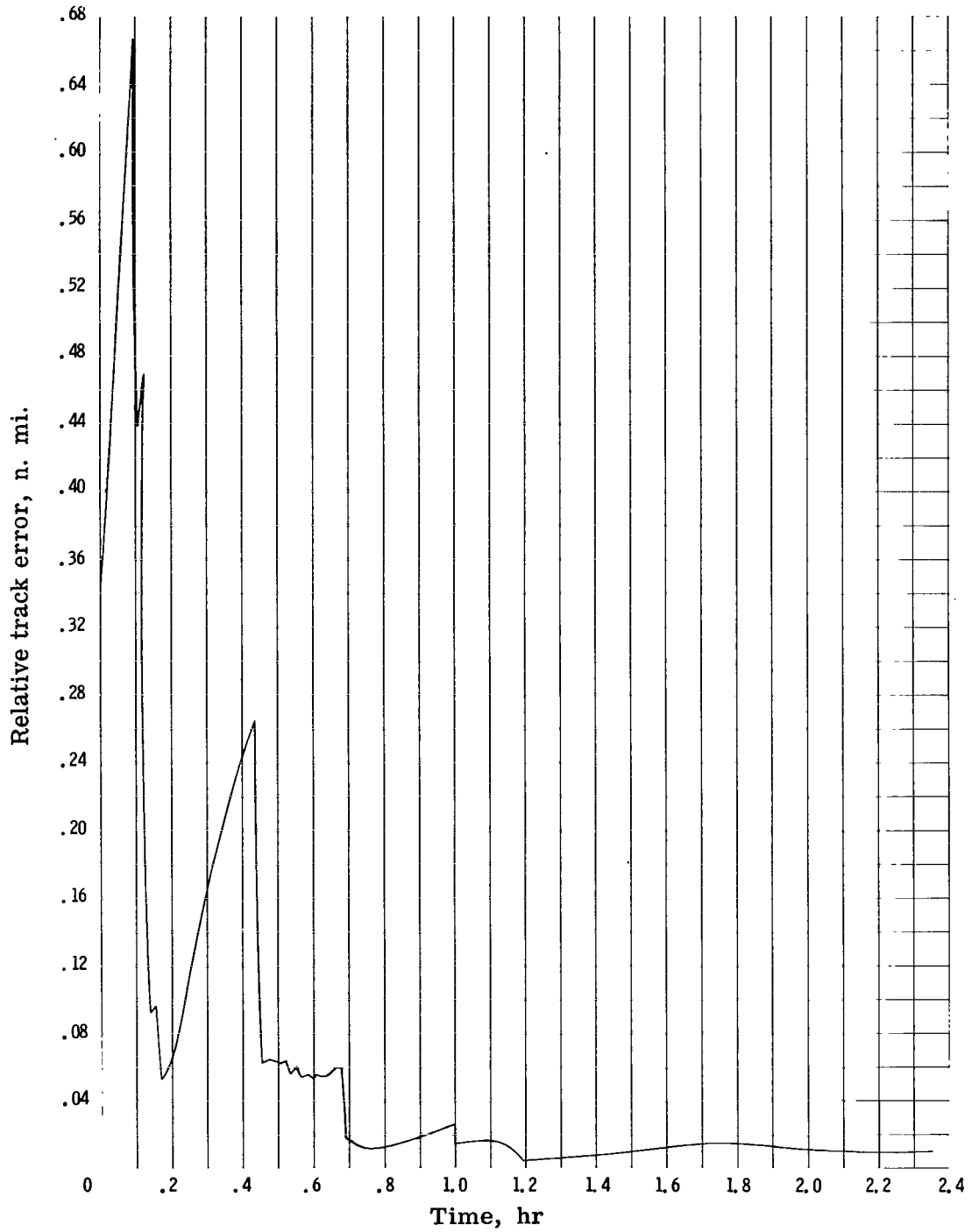
(a) Relative altitude error.

Figure 10. - Spacecraft-star measurements choosing stars nearest the measurement plane processed every 2 minutes up to circularization; spacecraft-lunar horizon measurements processed thereafter.



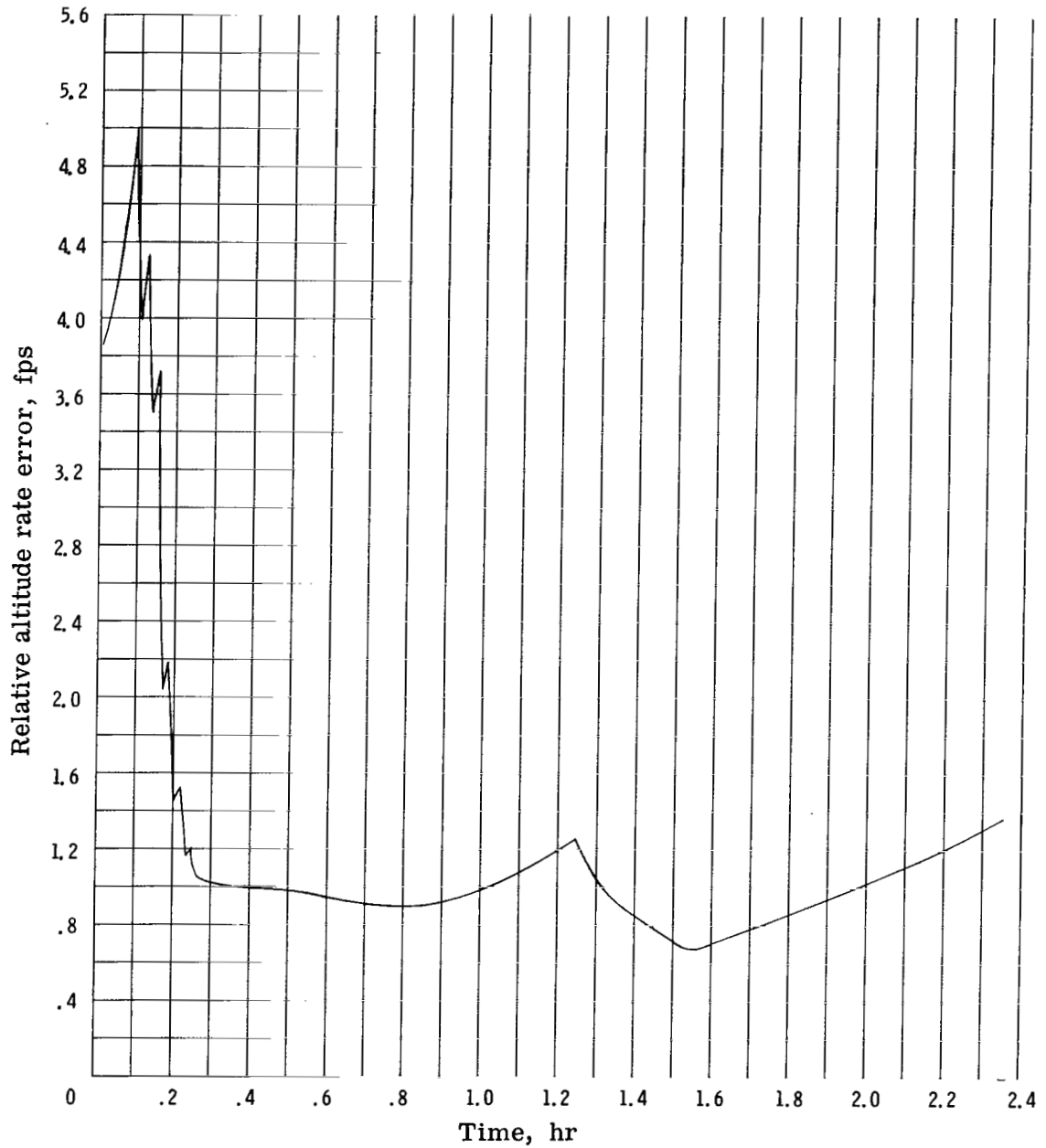
(b) Relative range error.

Figure 10. - Continued.



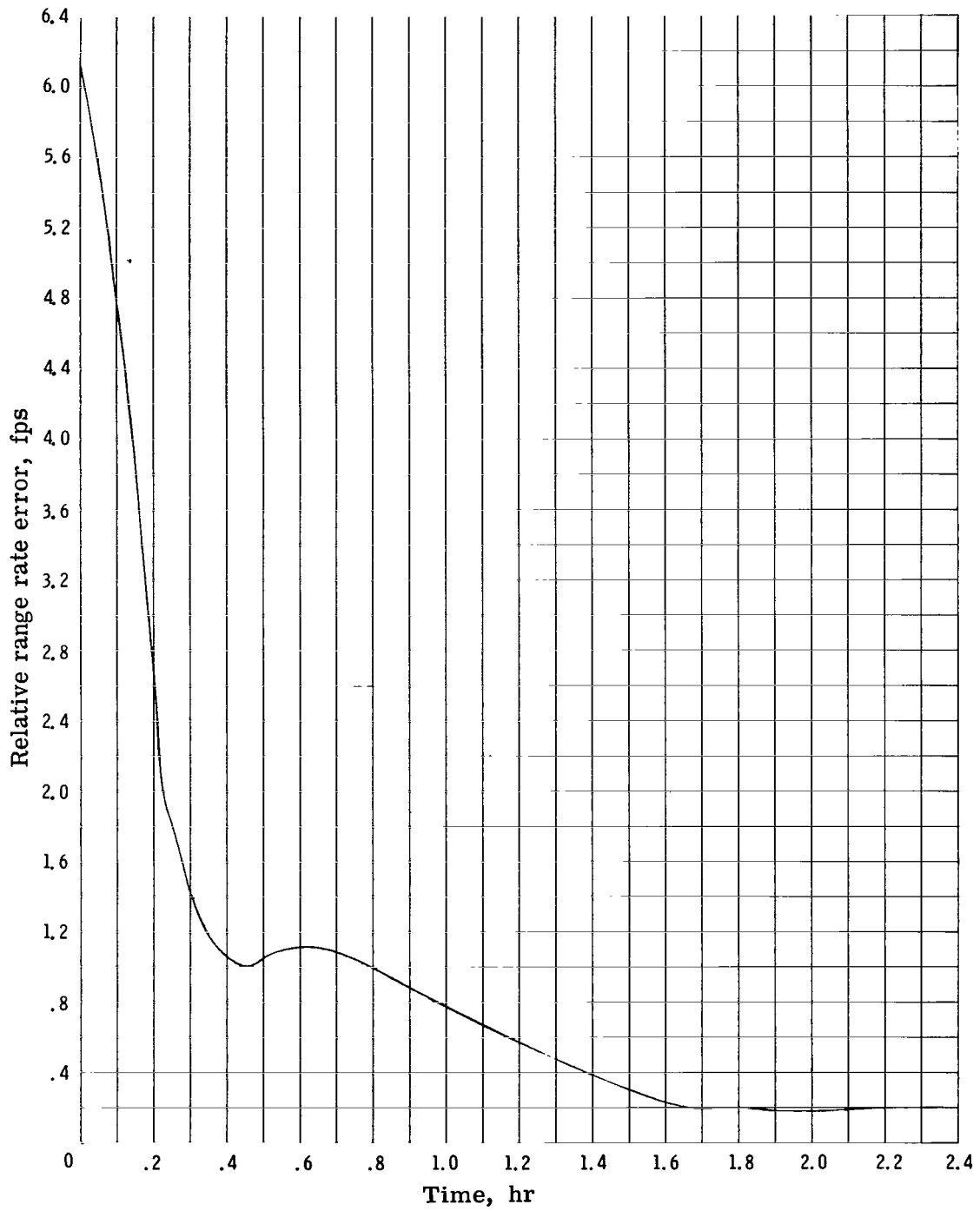
(c) Relative track error.

Figure 10.- Concluded.



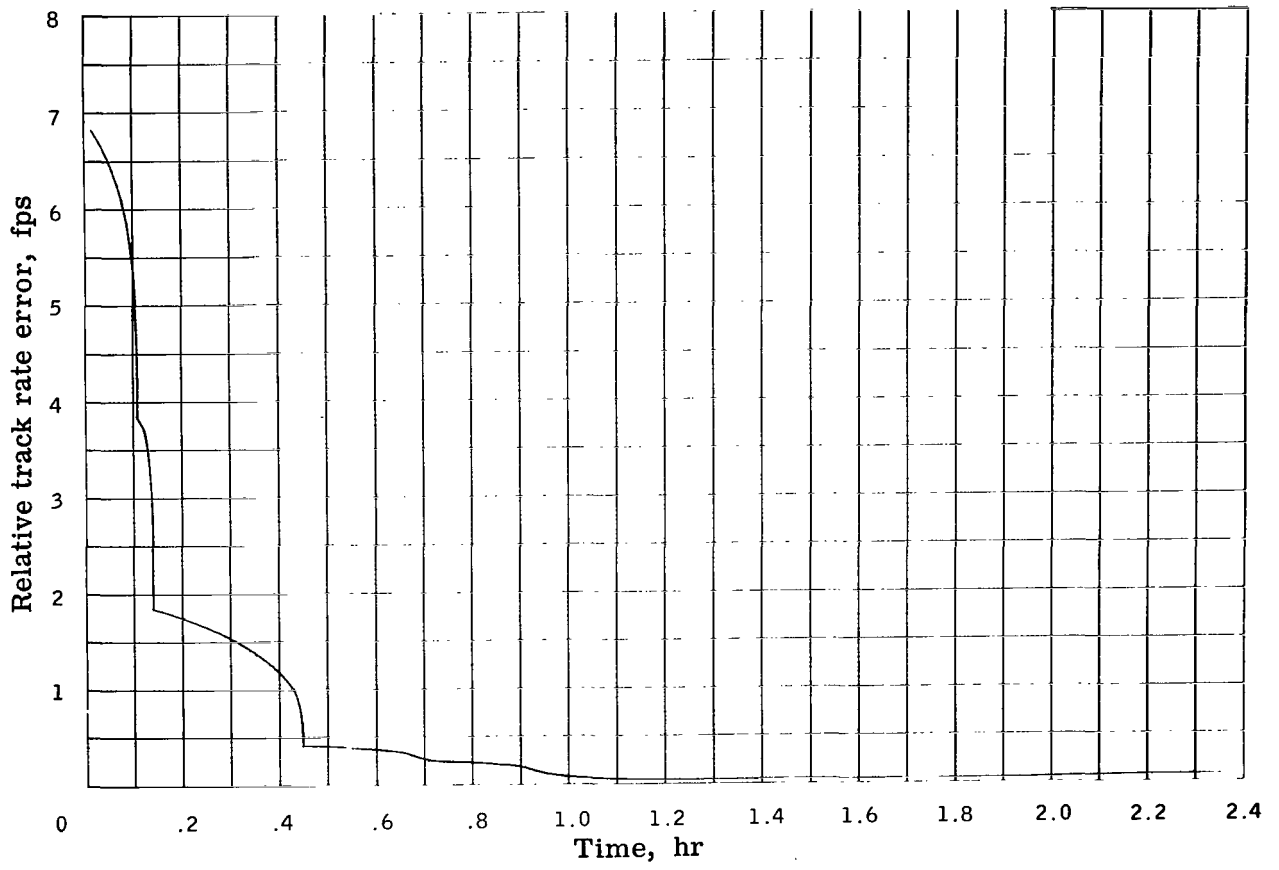
(a) Relative altitude rate error.

Figure 11.- Spacecraft-star measurements choosing stars nearest the measurement plane processed every 2 minutes up to circularization; spacecraft-lunar horizon measurements processed thereafter.



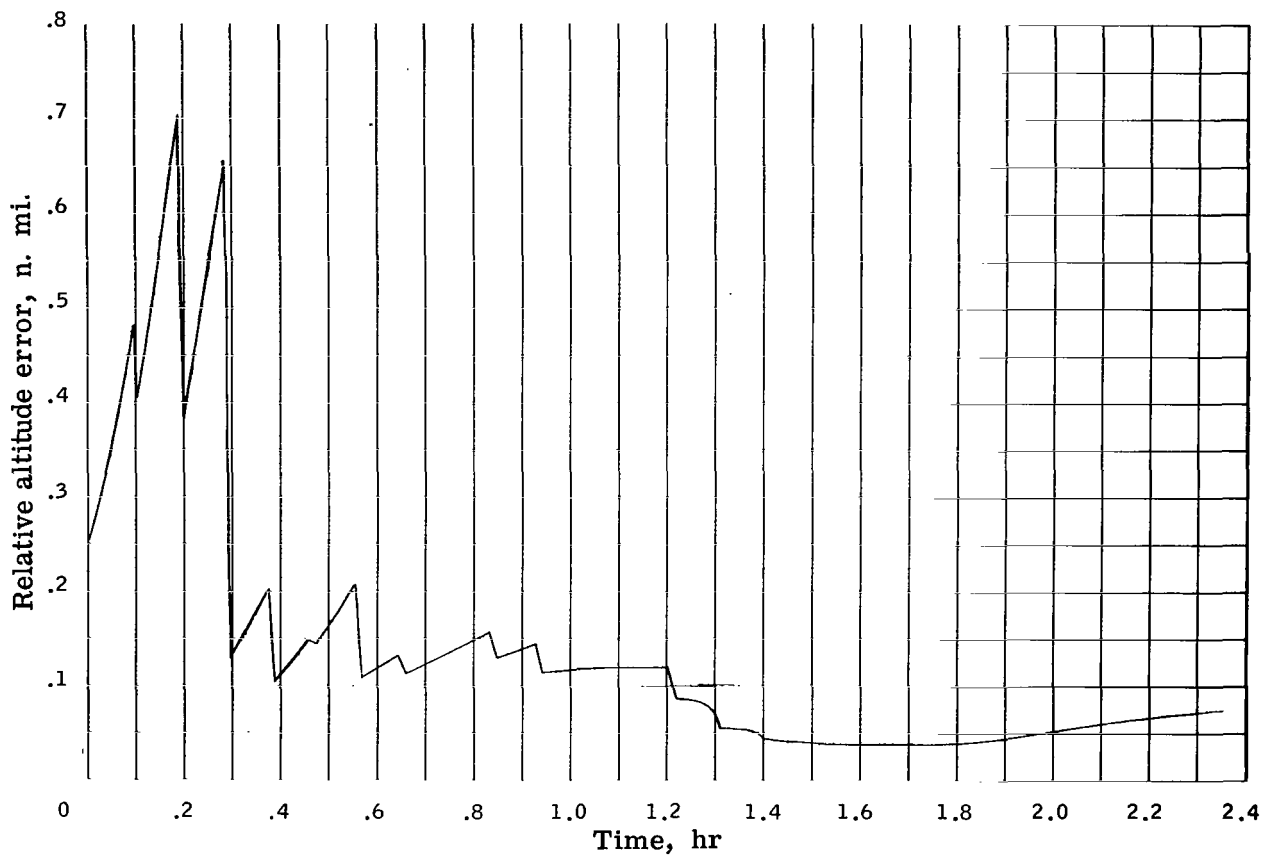
(b) Relative range rate error.

Figure 11.- Continued.



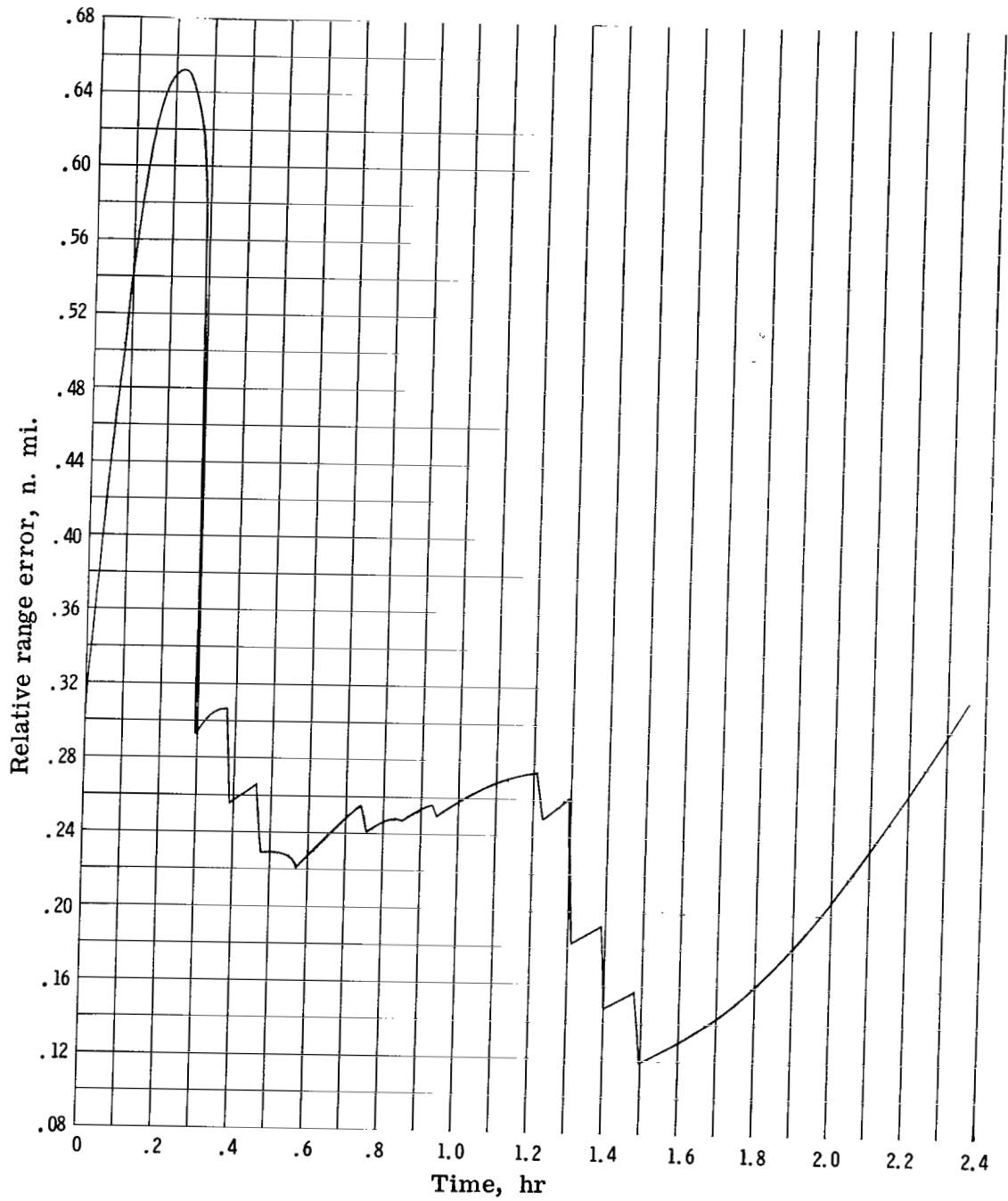
(c) Relative track rate error.

Figure 11. - Concluded.



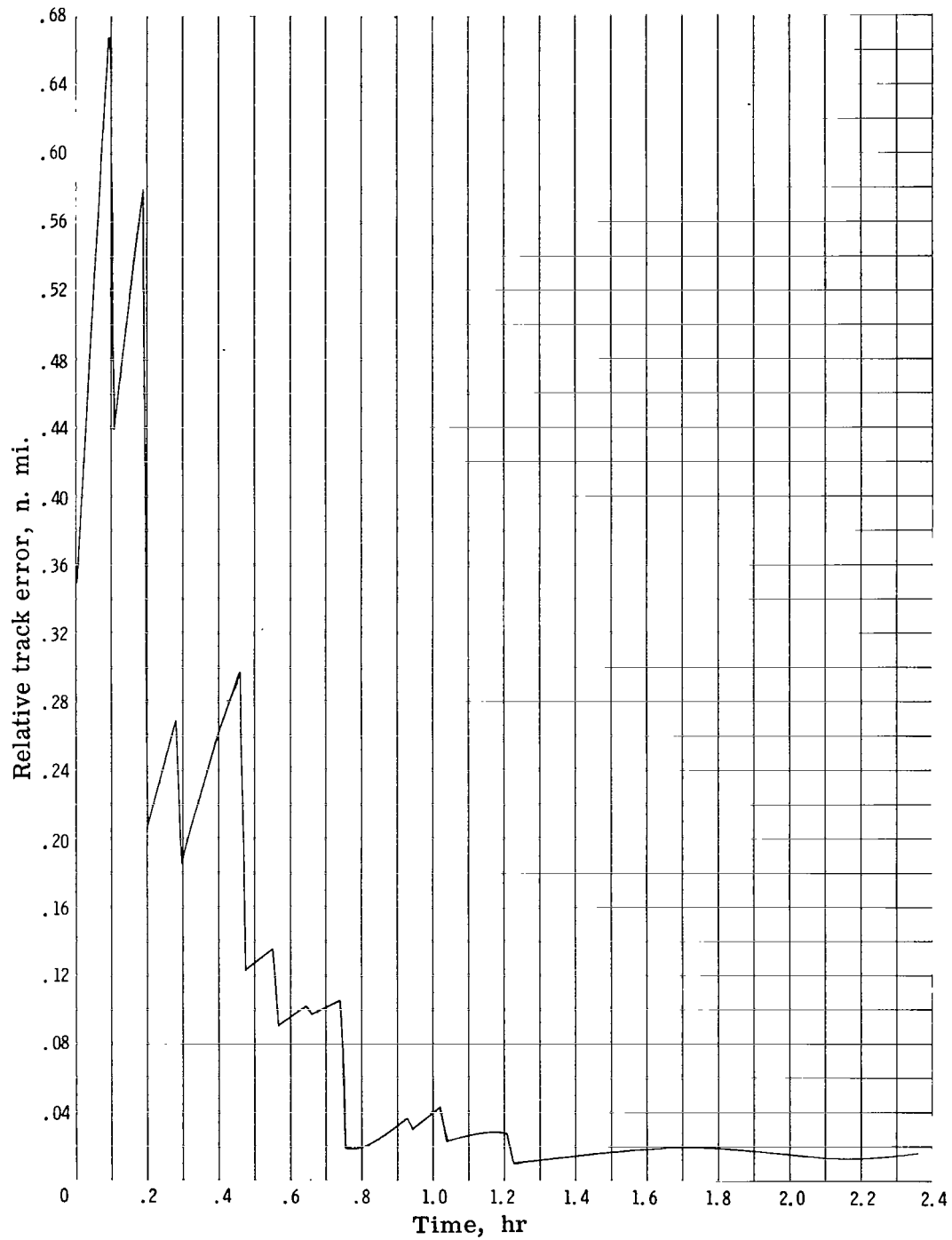
(a) Relative altitude error.

Figure 12. - Spacecraft-star measurements choosing stars nearest the measurement plane processed every 6 minutes up to circularization; spacecraft-lunar horizon measurements processed thereafter.



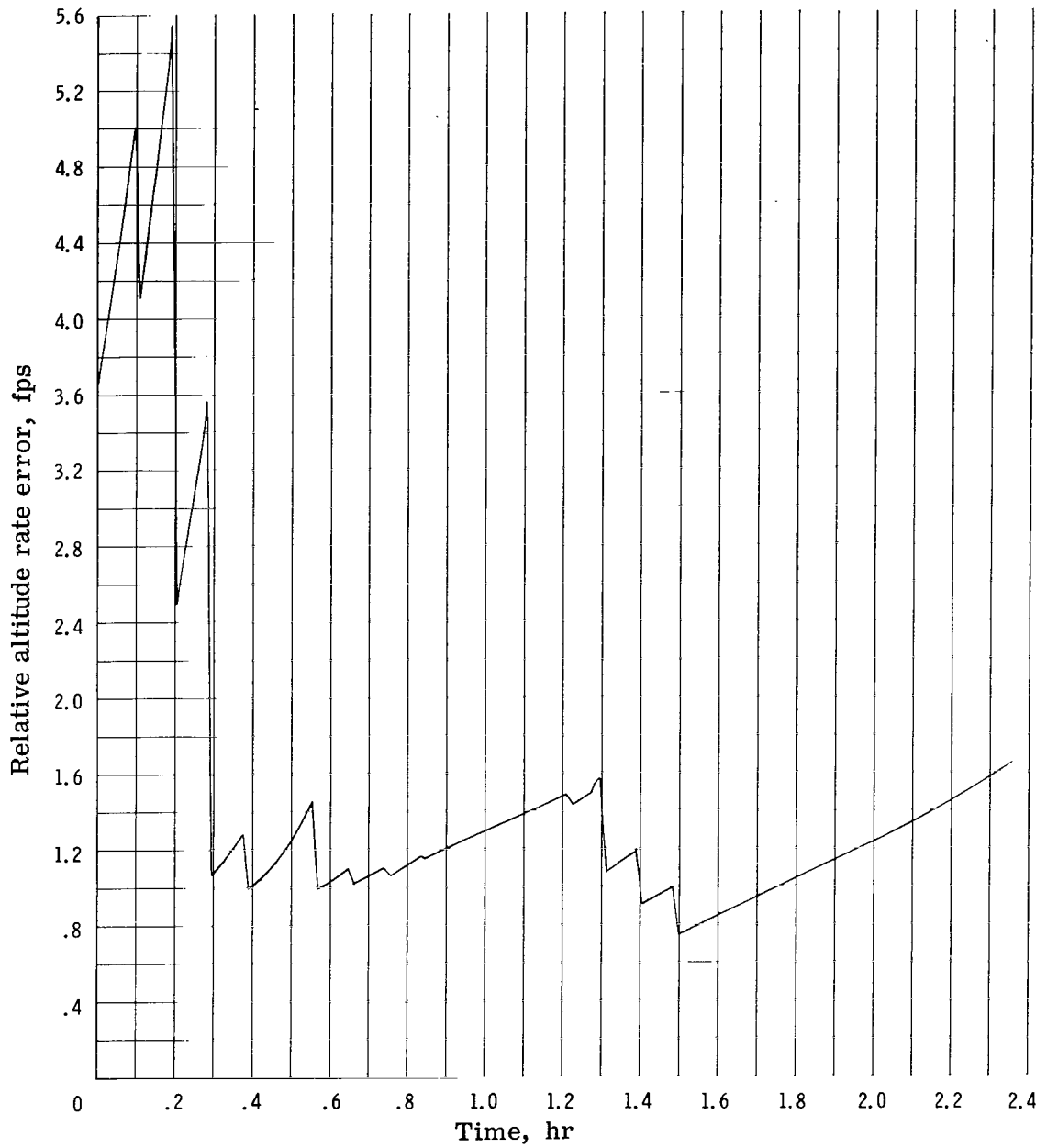
(b) Relative range error.

Figure 12. - Continued.



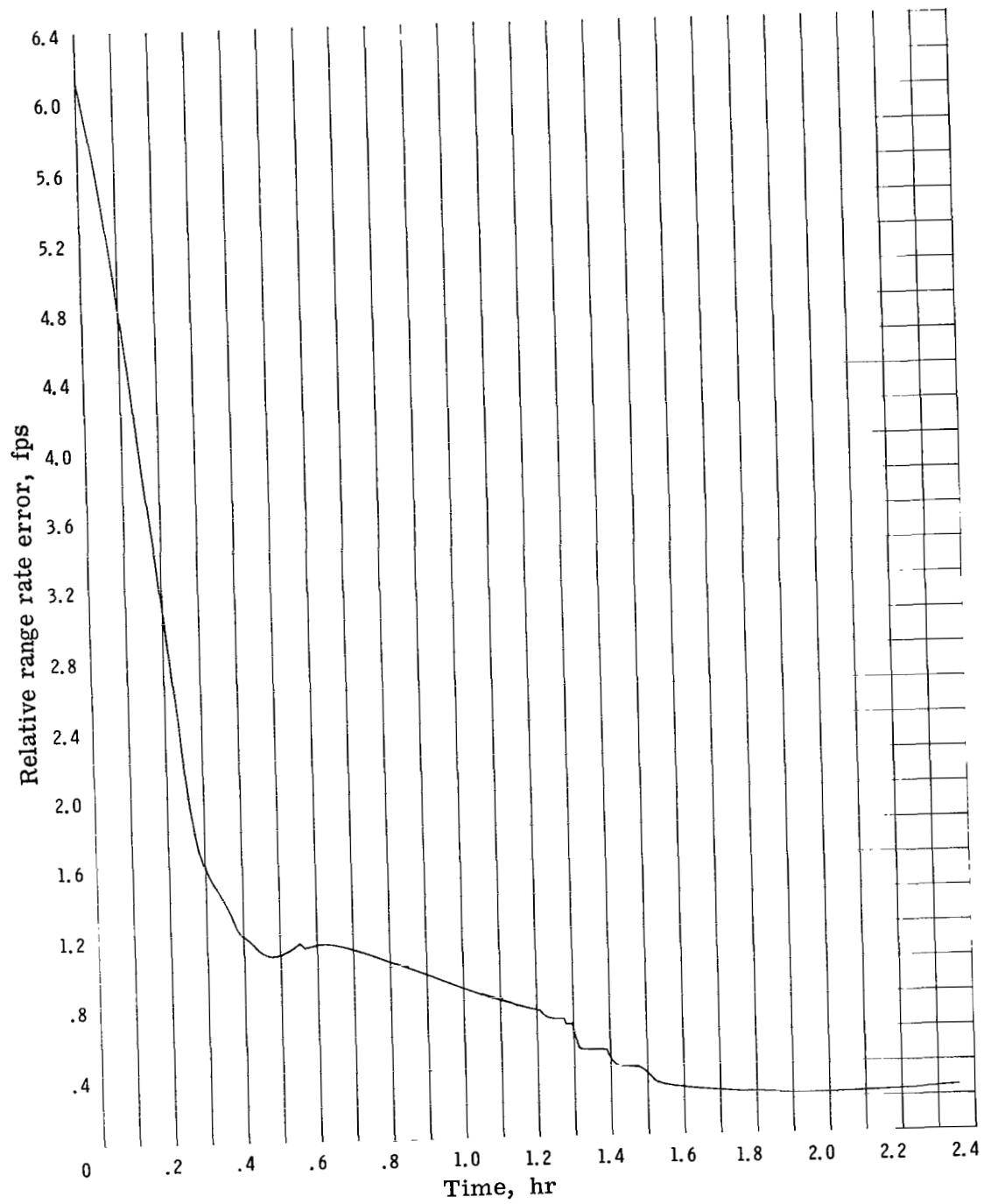
(c) Relative track error.

Figure 12. - Concluded.



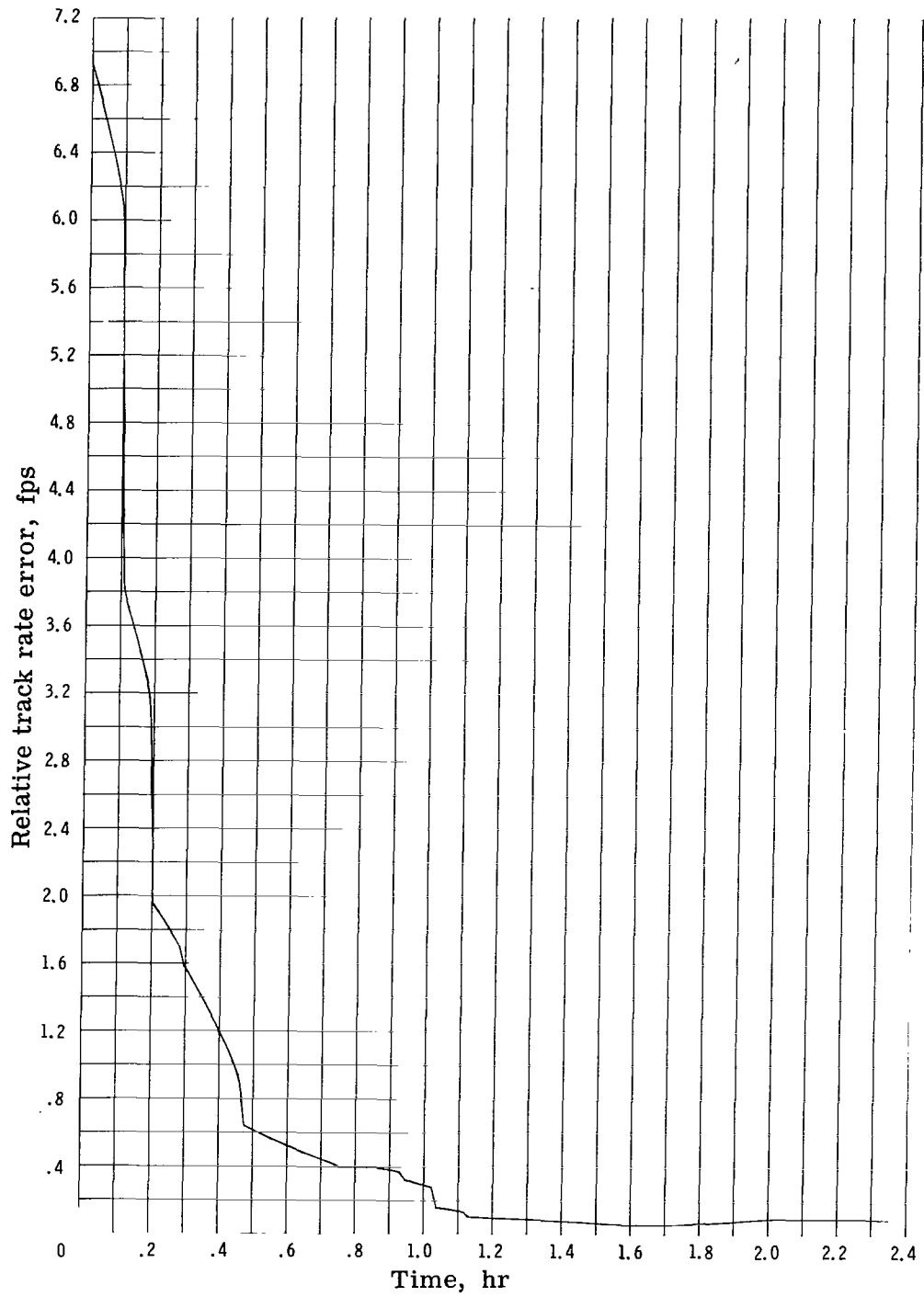
(a) Relative altitude rate error.

Figure 13.- Spacecraft-star measurements choosing stars nearest the measurement plane processed every 6 minutes up to circularization; spacecraft-lunar horizon measurements processed thereafter.



(b) Relative range rate error.

Figure 13. - Continued.



(c) Relative track rate error.

Figure 13. - Concluded.

"The aeronautical and space activities of the United States shall be conducted so as to contribute . . . to the expansion of human knowledge of phenomena in the atmosphere and space. The Administration shall provide for the widest practicable and appropriate dissemination of information concerning its activities and the results thereof."

—NATIONAL AERONAUTICS AND SPACE ACT OF 1958

NASA SCIENTIFIC AND TECHNICAL PUBLICATIONS

TECHNICAL REPORTS: Scientific and technical information considered important, complete, and a lasting contribution to existing knowledge.

TECHNICAL NOTES: Information less broad in scope but nevertheless of importance as a contribution to existing knowledge.

TECHNICAL MEMORANDUMS: Information receiving limited distribution because of preliminary data, security classification, or other reasons.

CONTRACTOR REPORTS: Technical information generated in connection with a NASA contract or grant and released under NASA auspices.

TECHNICAL TRANSLATIONS: Information published in a foreign language considered to merit NASA distribution in English.

TECHNICAL REPRINTS: Information derived from NASA activities and initially published in the form of journal articles.

SPECIAL PUBLICATIONS: Information derived from or of value to NASA activities but not necessarily reporting the results of individual NASA-programmed scientific efforts. Publications include conference proceedings, monographs, data compilations, handbooks, sourcebooks, and special bibliographies.

Details on the availability of these publications may be obtained from:

SCIENTIFIC AND TECHNICAL INFORMATION DIVISION
NATIONAL AERONAUTICS AND SPACE ADMINISTRATION

Washington, D.C. 20546